# A Linearized Prognostic Cloud Scheme in NASA's Goddard Earth Observing System Data Assimilation Tools

DANIEL HOLDAWAY

*Global Modeling and Assimilation Office, NASA Goddard Space Flight Center, Greenbelt, and Goddard Earth Sciences, Technology and Research, Universities Space Research Association, Columbia, Maryland*

RONALD ERRICO

*Global Modeling and Assimilation Office, NASA Goddard Space Flight Center, Greenbelt, and Goddard Earth Sciences, Technology and Research, Morgan State University, Baltimore, Maryland*

RONALD GELARO

*Global Modeling and Assimilation Office, NASA Goddard Space Flight Center, Greenbelt, Maryland*

JONG G. KIM

*Global Modeling and Assimilation Office, NASA Goddard Space Flight Center, Greenbelt, and Science Systems and Applications Inc., Lanham, Maryland*

RAHUL MAHAJAN

*Oak Ridge Associated Universities, NASA Postdoctoral Program, Oak Ridge, Tennessee, and Global Modeling and Assimilation Office, NASA Goddard Space Flight Center, Greenbelt, Maryland*

(Manuscript received 28 January 2015, in final form 16 June 2015)

ABSTRACT

A linearized prognostic cloud scheme has been developed to accompany the linearized convection scheme recently implemented in NASA's Goddard Earth Observing System data assimilation tools. The linearization, developed from the nonlinear cloud scheme, treats cloud variables prognostically so they are subject to linearized advection, diffusion, generation, and evaporation. Four linearized cloud variables are modeled, the ice and water phases of clouds generated by large-scale condensation and, separately, by detraining convection. For each species the scheme models their sources, sublimation, evaporation, and autoconversion. Large-scale, anvil and convective species of precipitation are modeled and evaporated. The cloud scheme exhibits linearity and realistic perturbation growth, except around the generation of clouds through large-scale condensation. Discontinuities and steep gradients are widely used here and severe problems occur in the calculation of cloud fraction. For data assimilation applications this poor behavior is controlled by replacing this part of the scheme with a perturbation model. For observation impacts, where efficiency is less of a concern, a filtering is developed that examines the Jacobian. The replacement scheme is only invoked if Jacobian elements or eigenvalues violate a series of tuned constants. The linearized prognostic cloud scheme is tested by comparing the linear and nonlinear perturbation trajectories for 6-, 12-, and 24-h forecast times. The tangent linear model performs well and perturbations of clouds are well captured for the lead times of interest.

## 1. Introduction

The linearized version of a weather forecast model is important for a number of reasons. Foremost it is central to the minimization algorithm used in four-dimensional

*Corresponding author address:* Daniel Holdaway, NASA Goddard Space Flight Center, Global Modeling and Assimilation Office, Code 610.1, Greenbelt, MD 20771.
E-mail: dan.holdaway@nasa.gov

DOI: 10.1175/MWR-D-15-0037.1

© 2015 American Meteorological Society

variational data assimilation (4DVAR), where it allows for a more optimal assimilation of time-evolving observations. A second and important use is in the adjoint-based observation impact tools, such as that used by the Global Modeling and Assimilation Office (GMAO) as well as a number of other weather centers (Gelaro et al. 2010; Lorenc and Marriott 2014; Langland and Baker 2004; Jung et al. 2013). A third application is as a research tool, for example, for estimating atmospheric sensitivity with the adjoint (e.g., Jung and Kim 2009) or to study singular vectors (e.g., Ehrendorfer and Errico 1995).

GMAO has recently implemented an updated linearized model based on the cube sphere finite-volume dynamics in the Goddard Earth Observing System, version 5 (GEOS-5). Physical parameterizations that can be enabled in the linearized model are a simplified boundary layer scheme, gravity wave drag, and the recently implemented convection and simple large-scale condensation moist physics schemes (Holdaway et al. 2014).

Including moist physics in the linearized model is known to be highly beneficial, especially for 4DVAR (e.g., Amerault et al. 2008; Errico et al. 2007; Errico and Raeder 1999; Janisková et al. 1999b; Lopez and Moreau 2005; Mahfouf and Rabier 2000; Stiller and Ballard 2009; Stiller 2009; Tompkins and Janiskova 2004). Since only a simple large-scale condensation scheme was implemented by Holdaway et al. (2014) some of these benefits could not be realized. For example, that linearized model provided no support for the evolution of perturbations of the cloud variables. Instead all supersaturation resulting from the dynamical evolution or from convective detrainment was assumed to be rained out to the surface within one time step. Although the simplified approach provided benefit in the context of improving observation impacts, the inclusion of a full linearized cloud model will offer greater improvement. Importantly the linearized cloud scheme will provide a framework for the assimilation of observations affected by moisture, such as those from the Global Precipitation Measurement (GPM) instrument (Hou et al. 2008).

The primary challenge in developing the tangent linear and adjoint versions of cloud models is that they are generally highly nonlinear. The physical parameterizations make use of many numerical switches and often employ functions with considerable variation. If these schemes are to be represented in a linear way then they must be carefully analyzed for nonlinearity and steep gradients in the underlying functions. Steep gradients can be particularly problematic for linearized models, which likely lack the proper description of some limiting on the quantity. Some effort is normally required to adapt the scheme to control any issues that arise, though invariably there is a trade-off. Any changes to the scheme will likely result in a degradation of the linear perturbation trajectory when compared with the nonlinear perturbation trajectory. Modifications toward linearity need to be balanced against the loss of accuracy.

Tompkins and Janiskova (2004) developed a linearized cloud scheme for use in the European Centre for Medium-Range Weather Forecasts (ECMWF) 4DVAR system. To simplify matters they developed a diagnostic version of the scheme, which they found to compare well to the full nonlinear model in terms of cloud cover. A similar diagnostic approach was tested against the nonlinear cloud model in GEOS-5, but was not found to perform particularly well. Much effort has been directed toward developing a prognostic approach to cloud modeling. The advective and diffusive effects are considered important for capturing the proper cloud characteristics. Given that producing a suitable diagnostic approach would require significant development and will not be able to account for advection and diffusion, a prognostic approach is implemented and tested here.

The cloud model used in GEOS-5 is that analyzed in Bacmeister et al. (2006). The scheme can be considered a single-moment microphysics scheme. It models the development and then removal (through precipitation and evaporation) of large-scale and anvil species of cloud liquid water and cloud liquid ice. Large scale refers to clouds formed through large-scale processes, such as dynamical convergence and upwelling. Anvil refers to clouds formed through detraining convection. The basis for the linearized cloud scheme is the full nonlinear cloud scheme, as used in GEOS-5. Much of the scheme is well suited to being linearized and perturbation growth is realistic. However, the part of the scheme that models the formation of clouds through large-scale condensation is not well suited to linearization. The scheme uses a probability density function (PDF) of total water in the grid box to model the fraction of large-scale cloud. The approach employs frequently applicable numerical switches and functions with very steep gradients with respect to the model state.

Two approaches are developed for handling the issues that occur concerning the calculation of large-scale cloud fraction. For data assimilation applications a so-called "perturbation model" is implemented in place of the current PDF method. This meets the efficiency requirements of 4DVAR, which requires many integrations of the tangent linear and adjoint models, while maintaining a close agreement between the linear and nonlinear perturbation trajectories. Currently a 6-h window is used for data assimilation at GMAO. For the 24-h integration, required for computing observation impacts and sensitivity studies, the global use of the perturbation model causes the linear and nonlinear perturbation trajectories to diverge too much. Only one or two integrations of the adjoint is required in

these applications so efficiency is less of a concern. As a result a filtering can be employed that examines the trajectory and determines whether or not the PDF approach will work well for the given grid box. Only in situations where it will cause problems is the perturbation model invoked.

The new linearized cloud model is tested by comparing the nonlinear perturbation trajectory with the linear perturbation trajectory. The accuracy of the tangent linear model is measured by examining spatial correlations, examining the perturbation fields by eye, and computing root-mean-squared errors. The performance of the efficient scheme is examined for 6- and 12-h forecasts. The performance of the scheme with filtering is examined for 24-h forecasts.

Stappers and Barkmeijer (2013) describe a Gaussian quadrature methodology for reducing the number of outer loops in 4DVAR. This method has been made available in the linearized version of GEOS-5 with a view to reducing the number of adjoint integrations required for the observation impact calculation (Gelaro et al. 2014). In GEOS-5 the observation impacts are typically computed using two adjoint sensitivity fields, obtained by separately linearizing around nonlinear forecasts initialized from the background and analysis fields. Instead the number of adjoint integrations is reduced to one by linearizing about the average of the background and analysis trajectories. In addition to providing a cost savings, the averaged trajectory approach maintains a higher than first-order approximation while only applying one sensitivity field. In fact, it appears to improve the accuracy over using the two sensitivity fields. Gelaro et al. (2014) have shown that the approach increases the percentage of the nonlinear observation impact that is captured by the linear estimate and extends the linearity assumption by 24 h. As a result it should be possible to calculate observation impacts for 48-h forecasts with the same accuracy that is currently seen for 24 h. The new linearized cloud scheme is tested with the Gaussian quadrature method.

The paper is arranged as follows. Section 2 outlines the development of the linearized prognostic cloud scheme and the development of the perturbation model and filtering. Section 3 shows the comparison of the linear and nonlinear perturbation trajectories for the new linearized physics routines. This section also examines the performance of the linearized moist physics with the newly available Gaussian quadrature and reduced trajectory read methods. Section 4 offers some conclusions.

## 2. Model description

In this section the formulation used for the linearized prognostic cloud scheme is described. The parts of the scheme that are problematic when linearized are outlined, as well as the efforts made to control these issues. The process by which perturbation cloud variables are split into the different species is discussed and some changes that are made to the boundary layer scheme are noted.

### a. Prognostic cloud model description

Model variables are linearized as $u = u^{(r)} + u'$, where superscript $(r)$ and prime $(')$ denote the reference and perturbation parts of the variable, respectively. The tangent linear model describes the evolution of the perturbation part around the reference part. It is expressed mathematically as

$$\mathbf{y}' = \mathbf{M}\mathbf{x}', \tag{1}$$

where the vectors $\mathbf{x}'$ and $\mathbf{y}'$ are all of the input and output perturbation model variables, respectively, and $\mathbf{M}$ is the linearized version of the model. The adjoint model, which makes use of the conjugate transpose of the linearized model, is

$$\frac{\partial J}{\partial \mathbf{x}'} = \mathbf{M}^{\mathrm{T}} \frac{\partial J}{\partial \mathbf{y}'}. \tag{2}$$

Note that the adjoint model propagates sensitivities with respect to the perturbation variables backward in time and relies on the choice of a cost function $J(\mathbf{y}')$. The tangent linear model propagates perturbations forward in time. The development of $\mathbf{M}$ is rather more straightforward than the development of $\mathbf{M}^{\mathrm{T}}$. The adjoint first requires a forward integration to provide the model trajectory at the correct time. Either the nonlinear model can be integrated and variables saved in strategic places, so-called check pointing (Charpentier 2001), or they can be recomputed as required. Usually some combination is employed as memory and efficiency requirements dictate.

The prognostic variables for the tangent linear model are zonal and meridional wind $u'$ and $v'$, potential temperature $\theta'$ (output as virtual temperature $T'_v$), specific humidity $q'$, pressure $p'$, cloud liquid water $q'_l$, cloud liquid ice $q'_i$, and ozone $\mathrm{O}'_3$. In the previous version of the linearized model, which supported only convection and simplified large-scale condensation, cloud liquid water and cloud liquid ice were, like ozone, purely tracers; no physics modified their values. With the addition of the physics described in this paper cloud liquid water and cloud liquid ice will be modified.

The nonlinear model does not have $q_l$ and $q_i$ as prognostic variables. Instead the variables that are carried are "large-scale" (resolved) and "anvil" (detraining convection) cloud species of each $q_{l,\mathrm{LS}}$, $q_{l,\mathrm{AN}}$, $q_{i,\mathrm{LS}}$, and $q_{i,\mathrm{AN}}$. In addition it carries the cloud fraction of each species $C_{\mathrm{LS}}$ and $C_{\mathrm{AN}}$. Each of these six variables are

subject to advection by the large-scale dynamics and all except cloud fractions are subject to turbulent diffusion by the boundary layer scheme. Variables are kept separate in the nonlinear model to simplify the modeling of the various cloud processes. The time scale of anvil clouds, for example, may be faster than the time scale of the dynamically driven large-scale condensation. As a result a different algorithm should be employed for the evolution of each species. In practice there is little physical difference (other than appearance) between anvil and large-scale species of clouds. A satellite flying overhead and observing a grid box containing clouds in the infrared or microwave spectrum would be unable to distinguish between them. It would, however, be able to distinguish between cloud liquid water and cloud liquid ice.

The cloud scheme in use in the nonlinear model is that noted in Bacmeister et al. (2006). The scheme acts on one column of the atmosphere and has four main stages to it: first cloud sources (from convection and large-scale condensation), second the evaporation and sublimation of anvil cloud, third the conversion from cloud to precipitation, and fourth the falling and reevaporation of precipitation. Between each component the scheme checks for unrealistic values of clouds, making discrete corrections where necessary. During the precipitation phase of the scheme moisture can be transported from one model level to the next via falling rain or snow or reevaporation.

Through this section of the paper the long and involved cloud model is heavily summarized in order to highlight its general behavior and highlight where issues arise as a result of linearization. (A version of the nonlinear scheme close to that outlined here is available online at http://geos5.org/trac/.)

### 1) CONVECTIVE CLOUD SOURCE

The first cloud source is from detraining convection (anvil). This part of the cloud scheme is quite simple since most of the work is performed by the convection scheme. The convection scheme is the relaxed Arakawa–Schubert (RAS) scheme (Arakawa and Schubert 1974; Moorthi and Suarez 1992). The linearized version of RAS is described by Holdaway et al. (2014). The tendencies for the two species of anvil cloud are

$$\frac{\partial q_{l,\mathrm{AN}}}{\partial t} = \frac{(1-F_i)S_c}{m}, \quad \text{and} \tag{3}$$

$$\frac{\partial q_{i,\mathrm{AN}}}{\partial t} = \frac{F_i S_c}{m}, \tag{4}$$

where $t$ is time. Here $S_c$, given in units of $\mathrm{kg\,m^{-2}\,s^{-1}}$, is the convective condensation source, provided by RAS. Mass $m$ for the model layer is given by, $m = \Delta p/g$, where $\Delta p$ is the pressure thickness for the layer (in pascals) and $g = 9.8\ \mathrm{m\,s^{-2}}$. The fraction $F_i$ that is ice is given by

$$F_i = \begin{cases} 1, & \text{if} \quad T \le T_{\min} \\ \left[1 - \dfrac{(T - T_{\min})}{(T_{\max} - T_{\min})}\right]^{I_p}, & \text{if} \quad T_{\min} < T \le T_{\max} \\ 0, & \text{if} \quad T > T_{\max}, \end{cases} \tag{5}$$

where $T$ is the temperature, $T_{\min} = 233.16$ K, $T_{\max} = 273.16$ K, and $I_p = 4$. Equation (5) is used considerably throughout the cloud scheme when splitting from total cloud liquid to the water and ice phases. Note that the function is discontinuous at $T = T_{\min}$ and $T = T_{\max}$. The default setting is $I_p = 4$, which makes the function nonlinear but smoother across $T = T_{\max}$ compared to smaller values of $I_p$. Using $I_p = 1$ would make it piecewise linear, which could be used to improve performance if necessary.

The anvil fraction tendency is calculated as

$$\frac{\partial C_{\mathrm{AN}}}{\partial t} = \frac{D}{m}, \tag{6}$$

where $D$ is the detraining mass flux from RAS, in units of $\mathrm{k\,gm^{-2}\,s^{-1}}$.

In implementing the linearized RAS scheme in GEOS-5, Holdaway et al. (2014) placed significant effort into controlling steep gradients and producing linear behavior. Since the detraining mass flux term comes directly from the central part of the RAS scheme, which is used to update the main variables, the perturbations of convective cloud source should be realistic and well behaved. Some nonlinearity occurs around the fraction of ice but it should not cause significant issue and perturbation growth should be realistic everywhere. Numerical testing confirms this hypothesis.

### 2) LARGE-SCALE CLOUD SOURCE

The large-scale cloud source is a rather complex iterative procedure. The approach is similar to that used in many AGCMs (e.g., Tiedtke 1993). The total water in a grid box is assumed to have a distribution that can be described by a PDF. The default shape of the PDF in this scheme is a "top hat" uniform distribution; however, an option for a triangular shape also exists and this is included in the linearized model. The PDF formulation used in GEOS-5 is described by Molod (2012).

The top hat PDF is centered on $q_T$, the total water for the (nonanvil) grid box. The nonanvil grid box is a temporary construct, defined as the portion of the grid box not covered by anvil but then rescaled to assume no anvil is present. Converting between the original grid box and the one that assumes no anvil involves dividing

by the cloud fraction. This results in dividing by the square of the anvil cloud fraction in the linearized model. Care is taken to ensure this does not cause an issue when the value is very small.

Half the width of the PDF is defined as $\alpha = 1 - \mathrm{RH}_c$, where $\mathrm{RH}_c$ is the critical relative humidity for the grid box, computed using a Slingo and Ritter (1985) formulation. To improve the efficiency of the linearized cloud scheme, perturbations of pressure are neglected. This is found to have negligible impact. Perturbations $\alpha'$ are not computed since $\alpha$ is a function only of pressure.

The cloud variables are updated as

$$q^n_{i,\mathrm{LS}} = q^{n-1}_{i,\mathrm{LS}} + q^n_{\mathrm{LS}} F_i, \quad \text{and} \tag{7}$$

$$q^n_{l,\mathrm{LS}} = q^{n-1}_{l,\mathrm{LS}} + q^n_{\mathrm{LS}}(1 - F_i), \tag{8}$$

where superscript $n$ denotes the time step. The total large-scale cloud at the new time is

$$q^n_{\mathrm{LS}} = q^{n-1}_{\mathrm{LS}} + (q_{\mathrm{LS0}} - q^{n-1}_{\mathrm{LS}}) \times \left\{ 1 - \left[ C_{\mathrm{LS}}(1-\alpha) - \frac{q_{\mathrm{LS0}}}{q_s} \right] \frac{\partial q_s}{\partial T} \frac{L_c + F_i L_f}{c_p} \right\}^{-1}, \tag{9}$$

where $L_c = 2.4665 \times 10^6\,\mathrm{J\,kg^{-1}}$ is the latent heat of condensation, $L_f = 3.3370 \times 10^5\,\mathrm{J\,kg^{-1}}$ is the latent heat of fusion, $c_p = 1004.49\,\mathrm{J\,kg^{-1}\,K^{-1}}$ is the specific heat capacity, and $T$ is temperature. The newly formed clouds are

$$q_{\mathrm{LS0}} = \begin{cases} 0, & \text{if} \quad q_s > q_T + \sigma \\ C_{\mathrm{LS}} \dfrac{q_T + \sigma - q_s}{2}, & \text{if} \quad q_T - \sigma < q_s \le q_T + \sigma, \\ q_T - q_s, & \text{if} \quad q_s \le q_T - \sigma \end{cases} \tag{10}$$

where $\sigma = \alpha q_s$. Saturation specific humidity $q_s$ for the grid box is computed using a table lookup. The large-scale cloud fraction is

$$C_{\mathrm{LS}} = \begin{cases} 0, & \text{if} \quad q_s > q_T + \sigma \\ \dfrac{q_T + \sigma - q_s}{2\sigma}, & \text{if} \quad q_T - \sigma < q_s \le q_T + \sigma \\ 1, & \text{if} \quad q_s \le q_T - \sigma. \end{cases} \tag{11}$$

The conditionals in Eqs. (10) and (11) represent whether the PDF is completely to the left of the saturation specific humidity (clear), completely to the right (cloudy), or whether the saturation specific humidity lies somewhere within the PDF (partially cloudy).

Other than initial "clean up" of small values, Eq. (11) is the first time the large-scale cloud fraction $C_{\mathrm{LS}}$ appears in the scheme. As such it is approximately a diagnostic quantity and is treated as such in the linearized model. Testing shows this to have negligible impact compared to treating it prognostically and represents a significant savings.

The use of discontinuities in the modeling of cloud sources can be particularly problematic. In nature the point of saturation is an equilibrium point. As supersaturation is reached cloud forms and precipitation occurs, pushing the atmosphere back to the threshold of supersaturation and the proximity of the discontinuity. As this repeats over time nonlinearity will build up. Unlike the discontinuity used in Eq. (5), the occurrence of values that are in close proximity to the discontinuity will be much more frequent.

In addition to nonlinearity, this part of the scheme also employs the use of functions with steep gradients, which can lead to unrealistic perturbation magnitudes. Consider Eq. (11), in the nonlinear model the cloud fraction is limited to being between 0 and 1. That means perturbations (difference between two nonlinear trajectories) are a maximum of 1. In testing the tangent linear model numerous grid boxes are identified as supporting values two and three orders of magnitude larger than this, quickly leading to very large cloud perturbations. The problems in this part of the scheme and the development of the remedy are discussed in section 2b.

In the nonlinear model Eqs. (9)–(11) are iterated three times. After each iteration the temperature is updated to account for phase changes and the associated heat exchange and then $q_s$ is updated. In the linearized version of this part of the scheme the number of iterations is reduced to one since iterative procedures are generally undesirable in a linearized model (Polavarapu and Tanguay 1998). Further, this prevents the additional burden required to save or recompute the reference solution when iterating the adjoint and reduces nonlinearity.

There are quite a few more steps within this part of the cloud scheme than shown here. Mostly these relate to separating the new clouds into the ice and water parts and balancing them with the temperature, specific humidity, and anvil clouds. These parts of the scheme do not result in spurious perturbation growth. However, throughout this process nonlinear checks are made to ensure only physically realistic values are present, which can add nonlinearity.

### 3) Evaporation and Sublimation

Once both cloud sources have been computed, evaporation of cloud liquid water to vapor and sublimation of cloud liquid ice to vapor are considered. This is only

done for the anvil species. The algorithms for evaporation and sublimation are identical, but using different constants. Central to the algorithm is the computation of the particle radius:

$$r = \left(\frac{q_e p}{NRT\rho_0^{4/3}\pi}\right)^{1/3}, \tag{12}$$

where $R = 287.00\ \mathrm{J\,kg^{-1}\,K^{-1}}$ is the gas constant for dry air and $\rho_0 = 1000\ \mathrm{kg\,m^{-3}}$. The constant $N$ and the variable $q_e$ differ between evaporation and sublimation. For evaporation $N = 50 \times 10^6$ and $q_e = q_{l,\mathrm{AN}}/C_{\mathrm{AN}}$; for sublimation $N = 5 \times 10^6$ and $q_e = q_{i,\mathrm{AN}}/C_{\mathrm{AN}}$. The linearized version of Eq. (12) will involve $T'$ and $q_e'$, which in turn involves the square of the cloud fraction. Generally the linearization of the radius calculation is found to behave well. However, when the anvil fraction gets quite small the division by its square can be problematic. The linearized version checks for when this occurs and adapts $q_e$ so that realistic magnitudes are produced.

### 4) AUTOCONVERSION

Autoconversion is the process by which cloud liquid water is converted to falling water and cloud liquid ice is converted to falling ice. The algorithms for anvil and large-scale species only differ in the constants.

The rain for the grid box is updated as follows:

$$q_{r,\mathrm{LS}}^n = q_{r,\mathrm{LS}}^{n-1} + q_{l,\mathrm{LS}}[1.0 - \exp(-R_p F_4 \Delta t)], \tag{13}$$

where $R_p$ is the rate of production. The constant $F_4$ is a height-dependent tuning constant used to reduce or increase cloud cover in specific regions. The formulation for $F_4$ contains nonlinearity through switches.

Functions involving an exponential can sometimes be problematic when linearizing. When the exponent is positive the gradient gets very steep and perturbations can quickly grow unrealistically large. In this instance $R_p$, $F_4$, and $\Delta t$ are all positive making the overall exponent negative. When the exponent is negative the gradient is small and the function is close to linear.

The production of snow from ice clouds is

$$q_{s,\mathrm{LS}}^n = q_{s,\mathrm{LS}}^{n-1} + q_{i,\mathrm{LS}}\frac{V_f \Delta t}{\Delta z}, \tag{14}$$

where $V_f$ is the settle velocity and $\Delta z$ is the vertical grid spacing. The settle velocity is computed using the formulation used by Lawrence and Crutzen (1998). For large-scale clouds the version they apply to regions outside of the tropics is used:

$$V_f = 109.0\left(\frac{q_{i,\mathrm{LS}}\rho}{C_{\mathrm{LS}}}\right)^{0.16}. \tag{15}$$

For anvil clouds the formulation they apply to the tropics is used:

$$V_f = 128.6 + 53.2\ln\left(\frac{q_{i,\mathrm{AN}}\rho}{C_{\mathrm{AN}}}\right) + 5.5\left[\ln\left(\frac{q_{i,\mathrm{AN}}\rho}{C_{\mathrm{AN}}}\right)\right]^2. \tag{16}$$

In Eqs. (15) and (16) $\rho$ is density calculated from the ideal gas law.

Care is required in the linearization of Eq. (15) since the power will reduce to something negative when differentiated. A numerical check on values $\leq 0$ is required. These functions have the potential to have steep gradients and nonlinearity due to the use of squares and logarithms. However, testing and examination of values reveals that the model lies within a linear regime of these functions and no issues with steep gradients are encountered.

### 5) PRECIPITATION AND REEVAPORATION

Three streams of precipitation fall toward the surface and reevaporate to the grid boxes above: large scale, anvil, and convective. Whereas the large-scale and anvil streams come from autoconversion the convective stream is output directly from the convection scheme. This stream represents precipitation inside the convective column and is protected from reevaporation to represent that it falls through a saturated convective tower. For each stream of precipitation both rain and snow are considered.

The precipitation routine first computes accretion and then reevaporation back to the levels above. The accretion of falling rain and snow follows Smith (1990):

$$(q_r)_k^n = (q_r)_k^{n-1} + 2[(q_r)_k^{n-1} + (q_r)_{k-1}^{n-1}]m_k(q_l)_k^{n-1}, \quad \text{and} \tag{17}$$

$$(q_s)_k^n = (q_s)_k^{n-1} + 2[(q_s)_k^{n-1} + (q_s)_{k-1}^{n-1}]m_k(q_i)_k^{n-1}, \tag{18}$$

where $k$ indicates the model level, increasing downward. The level mass is given by $m_k$. Between accretion and evaporation of precipitation the scheme allows for any phase changes to occur.

The evaporation and sublimation of rain and snow is computed as

$$(q_r)_k^n = (q_r)_k^{n-1}\exp\left[-\frac{V_r S_f \Delta z F_r^{-1}}{e_f D_r^2\left(1.0 + \frac{\partial q_s}{\partial T}\frac{L_c}{c_p}\right)}\right], \quad \text{and} \tag{19}$$

$$(q_s)_k^n = (q_s)_k^{n-1}\exp\left[-\frac{V_s S_f \Delta z F_s^{-1}}{e_f D_s^2\left(1.0 + \frac{\partial q_s}{\partial T}\frac{L_s}{c_p}\right)}\right]. \tag{20}$$

The evaporation for the convective stream is reduced using $S_f = 0.8$, for other streams $S_f = 1.0$. The variables $V_{r,s}$, $F_{r,s}$, and $D_{r,s}$ are the ventilation factor, fall velocity, and drop/flake size for rain and snow, respectively. The latent heat of sublimation is $L_s = L_c + L_f$. The term $e_f$ is

$$e_f = \frac{\rho_0 \left\{ \dfrac{L^2}{0.024 R_v T^2} + \dfrac{R_v T[\epsilon_i + (1-\epsilon_i) q_s]}{B_u q_s} \right\}}{\mathrm{RH}_c - q q_s^{-1}}, \quad (21)$$

where $R_v = 461.65\,\mathrm{J\,kg^{-1}\,K^{-1}}$ is the gas constant for water vapor, $B_u = 2.2$, and $\epsilon_i = R_v/R$.

After precipitation has been evaporated the quantities are saved to be combined with the level below during the next iteration of the loop. When coding the adjoint of the precipitation routine care is required to make sure the trajectory variables are available at the correct time, without excessive recomputation.

The functions used in the precipitation part of the scheme clearly have the potential to exhibit nonlinear behavior. The central part of the algorithm relies on an exponential with a negative exponent so large perturbation growth is not an issue. This is confirmed through testing of the numerical model. The degree to which nonlinearity affects the solution will be determined by fully examining the behavior of the tangent linear model.

The very final stage of the scheme is to remove residual supersaturation as well as any spurious negative specific humidity. These processes are done in a mass-conserving way. This clean-up has nonlinearity through the inherent use of discontinuities. Their inclusion in the linearized model does not appear to cause any issue, but is also found to have little benefit.

### b. Controlling the large-scale cloud source

To begin testing the linearization of the cloud scheme the tangent linear model is integrated using an analysis increment for the initial inputs. This provides initial perturbations with relevant magnitudes and structures. After one or two time steps, problems can be identified as appearing around the calculation of the large-scale cloud source. Values of the order of $C'_{\mathrm{LS}} = 500$ are identified during the first time step. As the integration progresses these large values quickly spread to the other cloud and thermodynamic perturbations. Within a few time steps, perturbations larger than can be computationally handled are encountered.

When problems occur, either due to large gradients or due to nonlinearity, there are generally two approaches that can be taken. First, the functions within the scheme can be altered before being linearized (the so-called perturbation model approach). Second, a filtering can be derived that seeks to locate problems and switch off the scheme or reduce the tendencies there. Each approach has distinct advantages and both come with challenges.

The challenge in finding an appropriate perturbation model is in identifying a function that suitably captures the behavior of the problematic function while eliminating the issues. The alternatives sometimes do not provide a linear perturbation trajectory that is close to the original nonlinear perturbation trajectory. On the other hand, developing a successful filtering is a highly arduous process, especially in identifying an appropriate aspect of the trajectory on which to filter. Filtering is generally the preferred approach since it preserves accuracy of the linear perturbation trajectory. However, it can be much more computationally intensive if no simple aspect of the trajectory can be identified.

Before attempting either approach it helps to simply place checks on the magnitude of the tangent linear perturbations, artificially reducing them to realistic values when a problem occurs. This provides a number of important insights. It ensures that every part of the model that has a problem is identified, it allows each problem to be worked on individually, and, most importantly, it provides a ceiling on how well the model can be expected to perform under use of filtering or a perturbation model. This also helps give a handle on the degree of linearity. The problems that occur around the large-scale cloud source scheme are diagnosed by determining when either $C'_{\mathrm{LS}}$, $q'_{l,\mathrm{LS}}$, or $q'_{i,\mathrm{LS}}$ go above a certain threshold, say the maximum seen for that level at that time in the nonlinear perturbation trajectory. Problems are generally quite infrequent, meaning a filtering approach should be obtainable.

From Eq. (11) one might suspect that problems occur due to some simple aspect of the trajectory, such as when the width of the PDF $\alpha$ gets very small. Figures 1a and 1b show scatterplots of a selection of nonzero cloud fraction and large-scale cloud liquid water perturbation increments produced by the large-scale cloud scheme versus the PDF width. The selection of points is taken from the first time step of the tangent linear model. It is clear that for these grid boxes large values of cloud fraction perturbations are fairly well correlated to small values of $\alpha$. This relationship does not hold for the largest perturbations of large-scale cloud liquid water increments though. Note that each panel shows a different set of grid boxes. Locations where cloud fraction perturbations are nonzero are not necessarily the same locations where large-scale cloud liquid water increment perturbations are nonzero.

Figure 1a shows how sometimes it is indeed possible to relate perturbation growth to some simple aspect of the trajectory. One could see how a filtering and perturbation model could be developed from examining

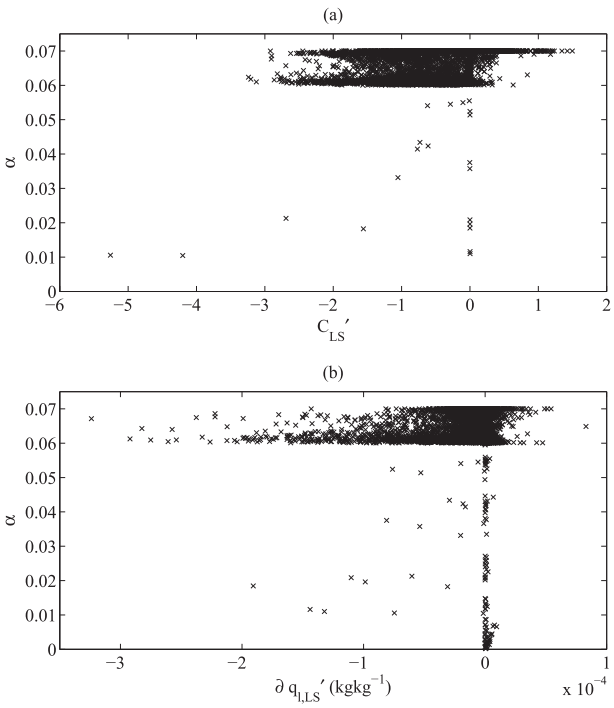


FIG. 1. A selection of (a) cloud fraction perturbation increments $\partial C'_{\mathrm{LS}}$ and (b) large-scale cloud liquid water perturbation increments $\partial q'_{l,\mathrm{LS}}$ scattered against the PDF width $\alpha$ for that grid box.

this relationship. Unfortunately the relationship seen for the selection of grid boxes shown in Fig. 1a begins to fail as more grid boxes and time steps are considered. Constructing a filtering that reduces cloud fraction when $\alpha < 0.055$ results in filtering a large number of grid boxes over a 6-h integration, many of which are important.

Numerous aspects of the trajectory have been examined against perturbation growth. Unfortunately no relationship can be found that holds when many grid boxes are considered. As a result, no simple filtering will be possible. It seems that problems can occur for a variety of reasons and be compounded by the prognostic nature of the scheme, which can cause small perturbation growth to amalgamate into large growth.

Since no simple measure of the occurrence of a problem can be constructed, filtering would have to be based on a measure of the overall behavior of this part of the cloud scheme. This is most simply achieved by examining the Jacobian, which can be used to understand the underlying behavior of the scheme (Holdaway and Errico 2014). This approach was used by Holdaway et al. (2014) and Errico and Raeder (1999) to control issues with the RAS convection scheme.

The RAS convection scheme is effectively one continuous algorithm with issues occurring throughout. Computing the Jacobian for the entire scheme was the most effective way of controlling issues with steep gradients. Here the Jacobian would only be computed for the cloud source. Despite this the added cost of computing even just specific columns of the Jacobian is not negligible.

Given the efficiency requirements of 4DVAR and that filtering based on the Jacobian is already required for the convection scheme adding further computations would not be ideal. As a result it is necessary to forgo the option to use filtering and the actual perturbation trajectory. Instead something that has good behavior by definition is used.

The general approach used here is to develop a simplified perturbation model that closely mimics the actual behavior for use in shorter, more efficient runs. For longer runs a filtering is developed that examines the Jacobian elements and eigenvalues. Then the perturbation model only needs to be called when a problem is deemed to occur. This helps keep the correlation between linear and nonlinear perturbations close for longer integrations.

In both cases the focus is on controlling the issues in the large-scale cloud source. However, this presents some other challenges to be considered during development. In the convection case, while simply turning off or reducing the effect of the linearized RAS scheme for a certain profile may not be ideal, it is physically sound. Conversely just switching off or reducing the large-scale cloud source for a certain grid box without also changing the sink parts may not be sensible. It would likely result in an unacceptable reduction in perturbations of clouds. An alternative approach might be to simply not compute the sinks part of the scheme once a problem is encountered in this source part. However, that raises the question of what effect that has on the grid boxes above and below through evaporation. The entire profile could be adapted, as done for the convection scheme, but that would likely result in almost all profiles being overadapted. Not simply turning off the cloud scheme or reducing the perturbation tendency, and instead using the perturbation model helps maintain cloud perturbation magnitudes.

### 1) PERTURBATION MODEL FOR CLOUD FRACTION

Figure 2a shows a scatterplot of the reference cloud fraction produced by Eq. (11) against the relative humidity for the grid box. It is clear that the cloud fraction produced by the PDF algorithm can be well represented by a simple underlying function of relative humidity. Given this relationship it should be possible to develop a simple perturbation model for the function. Shown on the figure are example piecewise linear and tanh function representations of the cloud fraction. The piecewise linear function gives a smaller overall error but contains discontinuities, the tanh function is smooth but has larger errors as well as steeper gradients. The gradients of both simplified

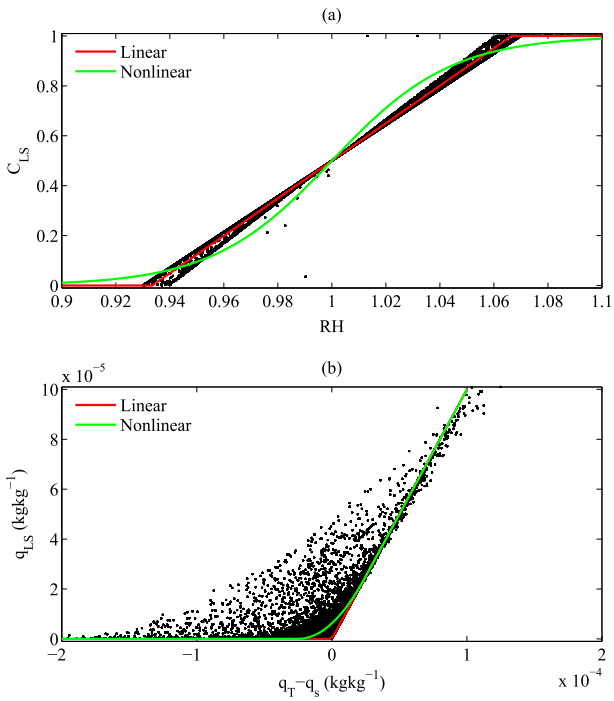


FIG. 2. (a) Correlation between the reference cloud fraction produced by the large-scale cloud source and the relative humidity for a selection of grid boxes. Also shown is a piecewise linear fit to the data (red curve) and a continuous nonlinear tanh fit (green curve). (b) Correlation between the reference large-scale cloud liquid water and the difference between the total nonanvil cloud liquid water and the saturation specific humidity for the grid box. Also show is a piecewise linear fit to the data (red curve) and nonlinear fit to the data (green curve).

functions are known and can be "regularized" by reducing to values that give perturbations with realistic values. Figure 2b shows a scatter of the large-scale cloud liquid water produced by Eq. (2) against $q_T - q_s$. Also shown is a piecewise linear function that is simply $q_{LS} = q_T - q_s$ when $q_T > q_s$ and 0, otherwise, and a nonlinear version that varies like $(q_T - q_s)^2$ close to the saturation threshold.

Using the simple piecewise linear function for calculating the cloud fraction perturbation is found to be the best option for the shorter data assimilation integration lengths. When using the perturbation model, before being linearized Eq. (11) is replaced with

$$C_{LS} = \begin{cases} 0, & \text{if} \quad \mathrm{RH} < c_1 \\ \dfrac{\mathrm{RH}}{c_2 - c_1} - \dfrac{c_1}{c_2 - c_1}, & \text{if} \quad c_1 \le \mathrm{RH} \le c_2 \\ 1, & \text{if} \quad \mathrm{RH} > c_2, \end{cases} \tag{22}$$

where $c_1 = 0.9335$ and $c_2 = 1.0665$. Note that the reference cloud fraction is computed using the regular PDF approach. For the linear function $\partial C_{LS}/\partial \mathrm{RH} = 7.52$ in the region $c_1 \le \mathrm{RH} \le c_2$, which is too large to give sensible perturbations. It is regularized to 1.50. This is a tuned value that is used in conjunction with reducing the tendency over the sinks to give realistic cloud perturbation magnitudes.

The function in Eq. (22), as well as the other functions shown in Figs. 2a and 2b, have been tested in place of the standard formulation in the nonlinear model. The replacement of the PDF approach for cloud fraction with the piecewise linear function in Eq. (22) results in an insignificant change to the cloud cover over a 24-h forecast. The piecewise linear function gives closer results to the original formulation than when using the tanh function. The functions fitted to the large-scale clouds produce realistic values when used in the nonlinear. However, the change is more significant than when the cloud fraction implementation is replaced.

With the cloud fraction perturbation given by the perturbation model, the large-scale cloud source part of the scheme is largely well behaved. A small change is made to Eq. (2) before it is linearized, becoming

$$q_{LS}^{n} = q_{LS}^{n-1} + \beta(q_{LS0} - q_{LS}^{n-1})\Psi^{-1}, \tag{23}$$

where $\Psi$ is the part of Eq. (2) in curly braces. The tuning parameter $0 < \beta \le 1$ can be used to control the growth of cloud perturbations, useful for runs longer than 6 h.

These changes, along with some minor changes to other parts of the cloud model, are sufficient to obtain realistic perturbations for the shorter 6- and 12-h integrations. For longer runs there is still some large perturbation growth and the accuracy of linear perturbation trajectories decline.

### 2) FILTERING FOR LONGER RUNS

The input and output variables for the large-scale cloud source scheme are $T'$, $q'$, $q'_{l,LS}$, $q'_{i,LS}$, $q'_{l,AN}$, $q'_{i,AN}$, $C'_{LS}$, and $C'_{AN}$. These are the variables that would make up the vectors $\mathbf{x}'$ and $\mathbf{y}'$ in Eq. (1) for this part of the model. The scheme works on a single grid box so inputs are rank one. Note that $C'_{LS} = 0$ in the inputs, so it does not need to be included in $\mathbf{x}'$. The matrix $\mathbf{M}$ in Eq. (1) is the Jacobian; expressions for each element can be determined by differentiating the functions that give the update of each variable, this can be seen in Holdaway and Errico (2014).

For a perturbation to undergo large growth through the time step requires large values to occur in the Jacobian. In some cases large growth can be identified from individual elements of the Jacobian. In other cases it may only be revealed from looking at eigenvalues. Note that computing the eigenvalues of the array adds cost.

Each column of the Jacobian is obtained by passing the tangent linear version of the scheme a 1 in place of the variable that the column multiplies and a 0 for all the other variables. So, for example, to obtain the first column, sensitivities with respect to $T$, the tangent linear scheme is passed $T' = 1$ and $q'$, $q'_{l,\mathrm{LS}}$, $q'_{i,\mathrm{LS}} = 0$. An approximation of the matrix could also be obtained using the nonlinear model.

It is clear from examining Jacobian elements (not shown) that there is correlation between the occurrence of large perturbation tendencies and large elements in the operator matrix. The relationship is clearest when comparing the column of the operator that multiplies temperature perturbations. For the parts of the array that multiply the other variables the grid boxes for which there is large growth are less distinct, often occurring when the magnitude of the array is relatively small. Generating the column of the array that multiplies the temperature perturbation only requires exercising the large-scale cloud source routine once. Tunable values, designed to filter no more than 20% of the grid boxes, are obtained and variables are filtered if values in the array exceed them.

If the entire $8 \times 8$ operator matrix is obtained for the grid box then the eigenvalues $\lambda$ can be computed. Before computing eigenvalues the Jacobian is adapted to represent the operator that would be derived from the tendency calculation, $\mathbf{A} = (\mathbf{A} - \mathbf{I})/\Delta t$. Eigenvalues are real and if $\lambda > 0$ then the magnitude of the perturbation grows through that time step. If $\lambda \gg 0$ then large, potentially unwanted, growth will occur. Even if $\lambda$ is only slightly larger than 0, but the operator does not change from one time step to the next then large growth can accrue over time. For the observation impact and sensitivity studies an option to filter grid boxes if $\lambda > 0.01$ helps to control perturbation growth and results in filtering fewer than 1% of grid boxes. Note that this adds significant cost over just computing the one column of the array that multiplies temperature perturbations.

Using this Jacobian filtering and then only calling the perturbation model when elements in the array or eigenvalues exceed certain thresholds is sufficient to give perturbation growth similar to that seen in the nonlinear model for a 24-h forecast. Doing nothing, or simply reducing the perturbation tendency, when thresholds are exceeded results in too much reduction of the cloud perturbations. Making use of the perturbation model is found to maintain realistic magnitudes for longer into the integration.

### c. *Splitting and storing of cloud variables*

Since the prognostic variables for the linearized model are $q'_l$ and $q'_i$ and the linearized cloud model requires $q'_{l,\mathrm{LS}}$, $q'_{l,\mathrm{AN}}$, $q'_{i,\mathrm{LS}}$, and $q'_{i,\mathrm{AN}}$, some method of splitting is required. This will also be true when an analysis of $q_i$ and $q_l$ is produced by the all-sky assimilation system. The assimilation system will not analyze the large-scale and anvil species separately. Instead the increments for $q_l$ and $q_i$ will need to be split before being used to adjust the model prognostic variables.

The perturbation variables are split into large-scale and anvil components by the ratio of large-scale to anvil found in the reference variables. In the all-sky assimilation the increment would be split with the same ratio that is found in the background. The dynamics and boundary layer routines in the linearized model will continue to see $q'_l$ and $q'_i$. In the module that calls the moist physics routines the two variables will be split into the four variables based on the trajectory ratio. At the end of the module the split variables will be combined. This approach was compared with keeping the variables separate in all parts of the linearized model. A negligible difference was seen between the approaches.

The cloud variables that must be available in the trajectory are $q_{i,\mathrm{LS}}$, $q_{l,\mathrm{LS}}$, $q_{i,\mathrm{AN}}$, $q_{l,\mathrm{AN}}$, and $C_{\mathrm{AN}}$. The minimum configuration of the linearized model requires $q_i$ and $q_l$ in the trajectory. This would represent an increase of three rank three variables in the trajectory. The trajectory read can be rather slow and require a large amount of memory for storage. Rather than store all four cloud species, just $q_{\mathrm{LS}}$ and $q_{\mathrm{AN}}$ can be stored in the trajectory and split into the liquid water and liquid ice parts using Eq. (5). A configuration of the model that uses just $q_{\mathrm{LS}}$ and $q_{\mathrm{AN}}$ in the trajectory was compared against storing all variables in the trajectory. A negligible difference was seen over a 24-h window. So, using $q_{\mathrm{LS}}$ and $q_{\mathrm{AN}}$ overall the number of variables read will only increase by one.

Two additional two-dimensional variables are added to the trajectory to be read in by the linearized model. The level index above and below where the eddy diffusivity $K_h > 2$. The fall speed of snow and ice is reduced where the boundary layer turbulence exceeds this threshold. Since eddy diffusivity is bell shaped storing just the level indexes is sufficient and saves recomputing $K_h$ or having to read an additional rank 3 variable.

### d. *Updated boundary layer physics*

The atmospheric planetary boundary layer plays a crucial role in the exchanges of heat and moisture between the surface and the atmosphere. Consequently a proper representation of the boundary layer in the linearized model is important in order to also produce realistic representation of cloud perturbations, especially in the lower atmosphere.

The simplified linearized boundary layer equation for potential temperature is

$$\frac{\partial\theta}{\partial t}=\frac{\partial}{\partial z}\left(K_h^{(r)}\frac{\partial\theta'}{\partial z}+K_h'\frac{\partial\theta^{(r)}}{\partial z}\right), \tag{24}$$

where $t$ is time and $z$ is height above the surface. The linearized eddy diffusivity is dependent on a stability function $f_h$, which is in turn dependent on the Richardson number, the ratio of buoyancy, and shear. The linearization of $K_h'$ is shown in Eq. (15) in Holdaway et al. (2013).

Currently the linearized version of GEOS-5 uses a very simplified eddy diffusion scheme and lacks a proper description of the planetary boundary layer. With the addition of the cloud scheme it is important to improve upon this by using the full form of $K_{m,h}^{(r)}$ that is used in the nonlinear model. This is done by recomputation, rather than storing in the trajectory. Issues arise with the inclusion of $K_{m,h}'$, specifically around the discontinuity when the Richardson number is zero (Janisková et al. 1999a). As such $K_{m,h}'$ terms are omitted here.

## 3. Model validation

In this section the tangent linear model with the new linearized cloud scheme is validated against its nonlinear counterpart. Both the nonlinear and tangent linear models are run at ½° resolution, using the cubed sphere grid (resolution is ≈55 km at the center of the cube faces). The time step of the nonlinear model is 450 s and the time step of the tangent linear model is 900 s. Smaller time steps for the tangent linear model have been tested but make a negligible difference to the solution. No change to the spatial or temporal resolution was found to negate the need for filtering in the cloud scheme. Tuning of the filtering is specific to a certain horizontal resolution though.

### a. Testing methodology

The performance of the tangent linear model is most easily assessed by comparing the nonlinear perturbation trajectory $M(\mathbf{x}+\delta\mathbf{x})-M(\mathbf{x})$ with the tangent linear perturbation trajectory $\mathbf{M}\delta\mathbf{x}$. Here $\delta\mathbf{x}$ represents some perturbation and $M$ represents the nonlinear model. Comparison between the nonlinear and linear perturbation trajectories is achieved using spatial correlations and root-mean-square difference (RMSE) at each model level and by contrasting the root-mean-square (RMS). As model output is on a latitude–longitude grid all of these metrics are area weighted to fairly measure both equatorial and polar grid boxes.

In practice the nonlinear and linear perturbation trajectories will not be equivalent, even for infinitesimal $\delta\mathbf{x}$. This is due to switches in the numerical code, missing physics in $\mathbf{M}$, discrepancies between the way the two models are set up and the extensive use of single precision numerics. In fact, choosing small $\delta\mathbf{x}$ can reduce the similarity between nonlinear and linear perturbation trajectories compared to a larger $\delta\mathbf{x}$. Switches can cause the nonlinear perturbations to get quite large, while the tangent linear perturbation would remain small. These issues are not particularly problematic since realistic choices of $\delta\mathbf{x}$ are not infinitesimal. Here a field similar to the analysis increment (background state minus analysis state) is used, $\delta\mathbf{x}=\mathbf{x}^b-\mathbf{x}^a$.

Examining the performance of the linearized moist physics has a number of challenges. Despite the importance of the moist physics schemes they are only strongly active at a relatively small number of grid points. Taking some global metric as the indicator of performance will likely under represent the moist physics. A complete measure of the performance of the linearized cloud model is only achieved by comparing and contrasting all the metrics for different regions of the globe and for regions where deep convection versus large-scale condensation is the dominant process.

The $M(\mathbf{x}^a+\delta\mathbf{x})=M(\mathbf{x}^b)$ nonlinear forecast is obtained by using the background field that would be provided to the data assimilation system as the model initial conditions. The $M(\mathbf{x}^a)$ forecast is obtained by using the analysis field (i.e., the field output from the data assimilation system) as the initial conditions. The analysis of the cloud variables is still in development so cloud variables in the initial conditions of the analysis forecast are not completely in balance with the other thermodynamic variables. For the background forecast they will be. In the first few model steps of the analysis forecast there will be a rapid adjustment, which may not be properly represented in the tangent linear model.

Rather than initializing the tangent linear model with the difference between the nonlinear model initial conditions (the analysis increment), it is initialized with the difference between the nonlinear models after a 3-h (24 time steps) "spinup" period. In all cases the incremental analysis update (IAU; Bloom et al. 1996) is switched off since it is not currently accounted for in the linearized model. Figure 3 shows a schematic of the background and analysis forecasts and the time at which the initial conditions for the tangent linear model are taken.

The linear perturbation trajectory is examined for 6-, 12-, and 24-h integrations, relevant for current and future data assimilation prospects and for observation impacts. To keep presentation simple, results shown below are for a single 24-h period, from 0300 UTC 1 February to 0300 UTC 2 February 2014. The runs begin and end at 0300 UTC to allow the 3-h spinup from the 0000 UTC analysis times. A month-long evaluation

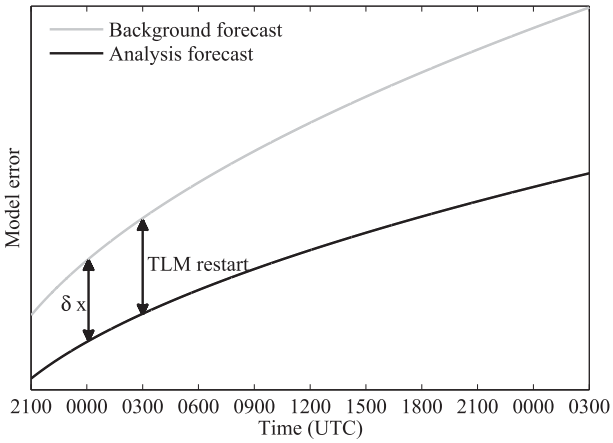


FIG. 3. Schematic showing the background and analysis forecasts and where initial conditions for the tangent linear model are taken.

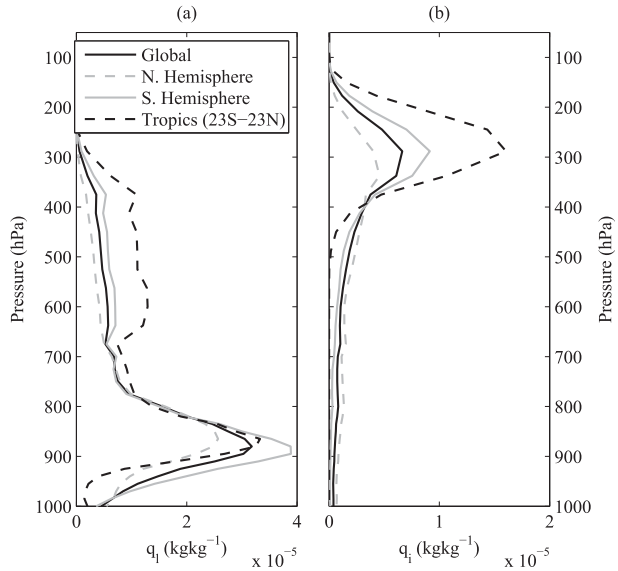


FIG. 4. The area mean for (a) $q_l$ and (b) $q_i$ at each model level.

for the whole of February, as well as days in other seasons (not shown) confirms similar results. A Northern Hemisphere winter case is chosen so as to provide a bias toward more large-scale condensation. Generation of large-scale condensation is nonlinear and needs substantial testing. Generation of very deep convection, as would be present in the Northern Hemisphere summer, is produced by the well-behaved RAS scheme, already extensively tested (Holdaway et al. 2014).

The adjoint model output is not explicitly analyzed here but its correct formulation is confirmed using the standard dot product test (Claerbout 2014). In all cases the addition of the cloud scheme does not degrade the number of decimal places to which the tangent linear and adjoint models agree. It should be noted, however, that the cloud scheme, and the previously implemented convection scheme, do not satisfactorily pass the dot product test unless all the calculations are performed using 64-bit arithmetic. To use these linearized moist physics schemes within a data assimilation minimization algorithm would require local double precision. This is possible in systems such as the Gridpoint Statistical Interpolation (GSI) analysis system used with GEOS-5.

Before examining the correlations for the cloud variables it is important to understand where the features are dominant. Correlations for the cloud fields that are close to 1 at a specific level, for example, tell us little about the overall performance of the scheme if there is negligible cloud cover at that model level.

Figure 4 displays the average cloud cover for $q_l$ and $q_i$, output from the 24-h analysis forecast. It is clear from the figure that for this time the majority of cloud liquid water exists between 780 and 950 hPa, where stratus clouds prevail. Cloud liquid ice exists predominantly between 200 and 400 hPa, where convection is detraining and creating cumulonimbus and anvil type clouds. The Southern Hemisphere, which has greater ocean fraction and is in summer, has more cloud cover than the Northern Hemisphere. The Northern Hemisphere has more extensive low-level ice clouds, where colder climates allow for its presence at lower altitudes. Near the South Pole, subsidence resulting from the strong katabatic winds over Antarctica generally results in very dry conditions. As a result low-altitude ice clouds in the Southern Hemisphere summer are almost nonexistent. Clouds in the extratropics result predominantly from large-scale condensation. Clouds in the tropics result predominantly from convection.

### b. *A note on linearized dynamics*

It should be noted that there are some important differences between the linearized dynamical core and the nonlinear dynamical core. More horizontal diffusion is used in the linearized model than in the nonlinear model, especially applied to temperature in the upper-level jet region. In this region large spurious perturbation growth, not seen in the nonlinear perturbation, is otherwise encountered. Additionally there are differences in the dynamical transport algorithms, discussed below. The effect of these changes, especially the extra diffusion, can be to reduce the magnitude of the perturbation fields when compared to the nonlinear model. This is an example of the kinds of compromises that are often necessary when linearizing complex models.

Clouds and ozone are tracers. They are subject to advection and vertical remapping of Lagrangian levels by the dynamics, but only affect other variables through the physics. Specific humidity has a small effect through

the dynamics, in the calculation of virtual temperature, but otherwise only has an affect through the physics. In the GEOS-5 nonlinear model tracers are advected and remapped using a piecewise parabolic method (PPM) with nonlinear flux limiter designed by Lin (2004). Other variables, such as wind and temperature, are also subject to some version of the flux limiter. Flux limiters are designed to maintain the shape of discontinuities and prevent the development of oscillations and other spurious numerical values, such as negative tracer values. To achieve this a nonlinear approach is unavoidable (Thuburn and Haine 2001). The steeper the horizontal gradients in the underlying field the more the flux limiters will be activated and the more nonlinear the solution will be. For the smoother wind and temperature fields use of the limiter will be considerably less than it will be for the discontinuous clouds. Neglect of such nonlinearity means that in the linearized model correlations for the clouds and specific humidity will generally be lower than the correlations seen for winds and temperature.

To develop an understanding of the impact of these nonlinearities a simple experiment was performed treating the cloud variables as passive tracers in both the linearized and nonlinear models. Under this scenario the moist physics are turned off and changes to clouds do not affect other variables. Even with this simplified setup the correlations of the cloud variables are considerably lower than for other fields. So even if the cloud processes were linear, correlations for cloud fields would remain lower than for other fields, due to the dynamics. The experiment was further simplified by turning off the flux limiters and turning off the vertical remapping. With this level of simplification the correlation for the cloud variables became similar to that seen for the other variables. Neither turning off the remapping nor simplifying the transport individually increased the correlations.

In addition to using a nonlinear formulation, the flux limiter used for advection also employs very steep gradients, which can cause problems when linearized. To prevent these problems from occurring the linearization of the flux limiter must be turned off in the linearized model. A simple third-order advection scheme is used for the clouds, specific humidity, and ozone. This kind of scheme, although well behaved in terms of perturbation growth, is not positive definite and does not prevent oscillations near discontinuities. For the perturbation fields this is an allowable compromise. For vertical remapping the linearization of the flux limiter is also turned off.

Motivated by the findings in this paper an investigation is ongoing to provide further understanding around the use of flux-limited advection schemes in the linearized dynamics.

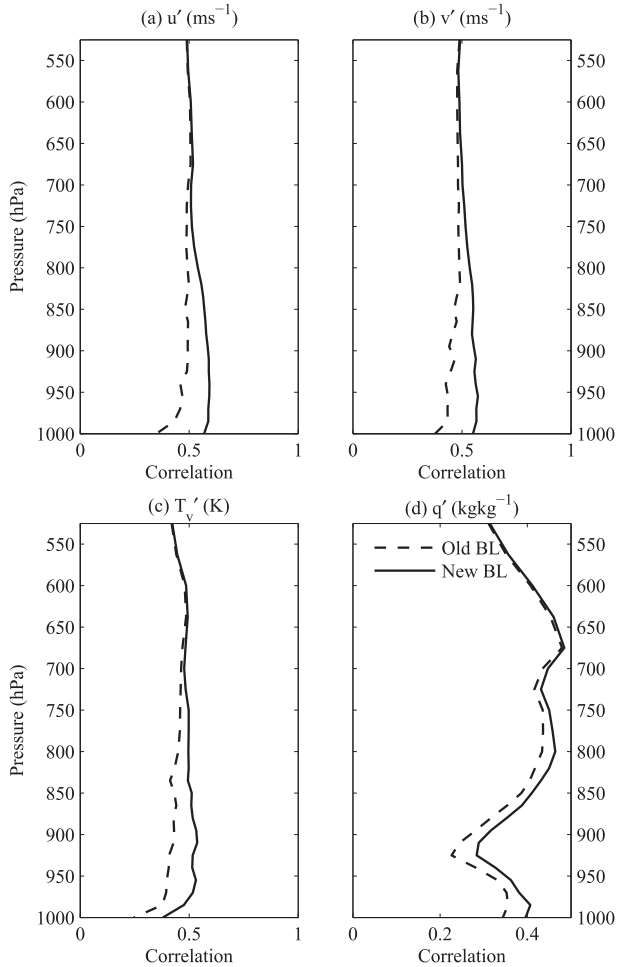


FIG. 5. The 24-h spatial correlations for (a) $u'$, (b) $v'$, (c) $T_v'$, and (d) $q'$ as a function of pressure.

### c. Boundary layer validation

Figure 5 shows the spatial correlation between the nonlinear perturbation and linear perturbation trajectory for a 24-h forecast. The correlations are computed at each level and plotted against pressure, up to approximately 500 hPa.

It is clear from Fig. 5 that when using the proper form of the reference boundary layer diffusion coefficients, rather than the old eddy diffusion scheme, the correlation is significantly improved. The biggest improvement is seen in the wind fields, where the average global correlation below 500 hPa increases from 0.48 to 0.55 for $u'$ and from 0.46 to 0.53 for $v'$. For virtual temperature it increases from 0.42 to 0.49, for specific humidity it increases from 0.37 to 0.39 and for the pressure thickness (not shown) it increases from 0.77 to 0.81. These improvements will provide the cloud scheme with more accurate thermodynamic perturbations as

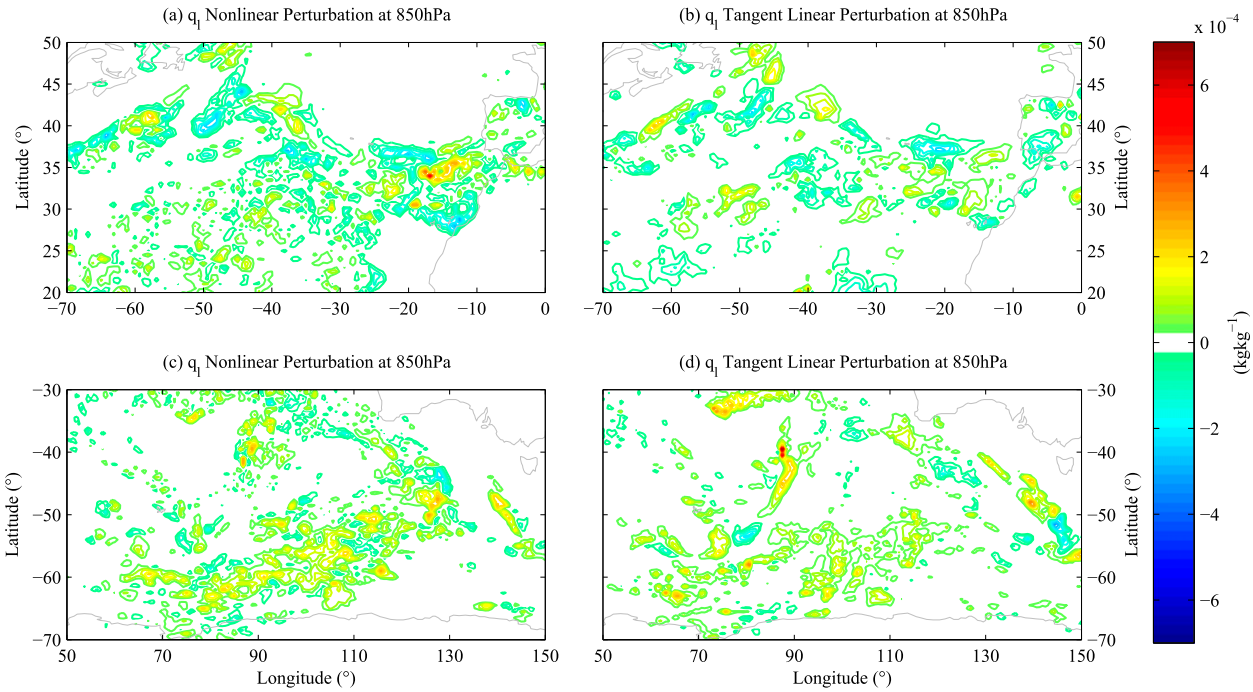


FIG. 6. Horizontal cross sections of the perturbations of cloud liquid water fields for a 6-h forecast. (a),(c) The nonlinear perturbation and (b),(d) the tangent linear perturbation. (a),(b) The perturbations for a region of the North Atlantic Ocean. (c),(d) A region of the southern Indian Ocean. The contour interval is $4 \times 10^{-5}$.

well as ensuring that linearized vertical diffusion of the cloud perturbations is more accurate.

### *d. Cloud scheme validation: 6- and 12-h forecasts*

This subsection discusses results from integrating the tangent linear model with the cloud scheme configured for data assimilation purposes. This is the more efficient method of handling of the cloud fraction and large-scale cloud source issues. Because of the nonlinearity of the model being considered, the linearized model will not capture every small-scale detail of nonlinear perturbations. The comparison begins by performing a qualitative check that the linearized model captures the correct kinds of perturbation structures and magnitude for specific regions. This is backed up with a quantitative check on correlations and root-mean-square errors.

Figure 6 shows the cloud liquid water perturbations for a 6-h integration. The model level shown is at approximately 850 hPa, the height for which cloud liquid water coverage is largest. Two specific regions are displayed, chosen for the extensive perturbations of cloud liquid water in those areas. Figures 6a and 6b compare the nonlinear and linear perturbation trajectories, respectively, over the northern Atlantic Ocean. Figures 6c and 6d show an area over the southern Indian Ocean.

Comparing Figs. 6a,c with 6b,d it is clear that much of the structure captured by the tangent linear model is also seen for the nonlinear model. This is despite the nonlinearity identified in the equations, and despite the fact that a different formulation of large-scale cloud formation is being used. The linearized model is producing perturbation structure located in qualitatively correct locations, with mostly similar magnitudes and sign as the nonlinear model. The use of a perturbation model, as well as increased horizontal diffusion, prevents spurious perturbation growth, but also prevents the linearized model capturing all of the small-scale structure seen for the nonlinear model. As a result, the linear perturbation trajectory is sparser than the nonlinear perturbation trajectory. Although magnitudes are mostly similar, they are overall a little smaller for the linearized model than the nonlinear model. In addition, there are highly localized large perturbation magnitudes that are seen in either the nonlinear or linear perturbation trajectory, without being present in the counterpart. The performance of the linearized model is similar for other regions and heights not shown here. In regions of the atmosphere where the nonlinear model does not produce any perturbation structure (not shown) the linearized model does not either.

Figure 7 shows perturbations of cloud liquid ice at 250 hPa for the 6-h integration. Regions shown here are over Australasia and Brazil, areas where perturbations of cloud liquid ice are widespread. As seen for the

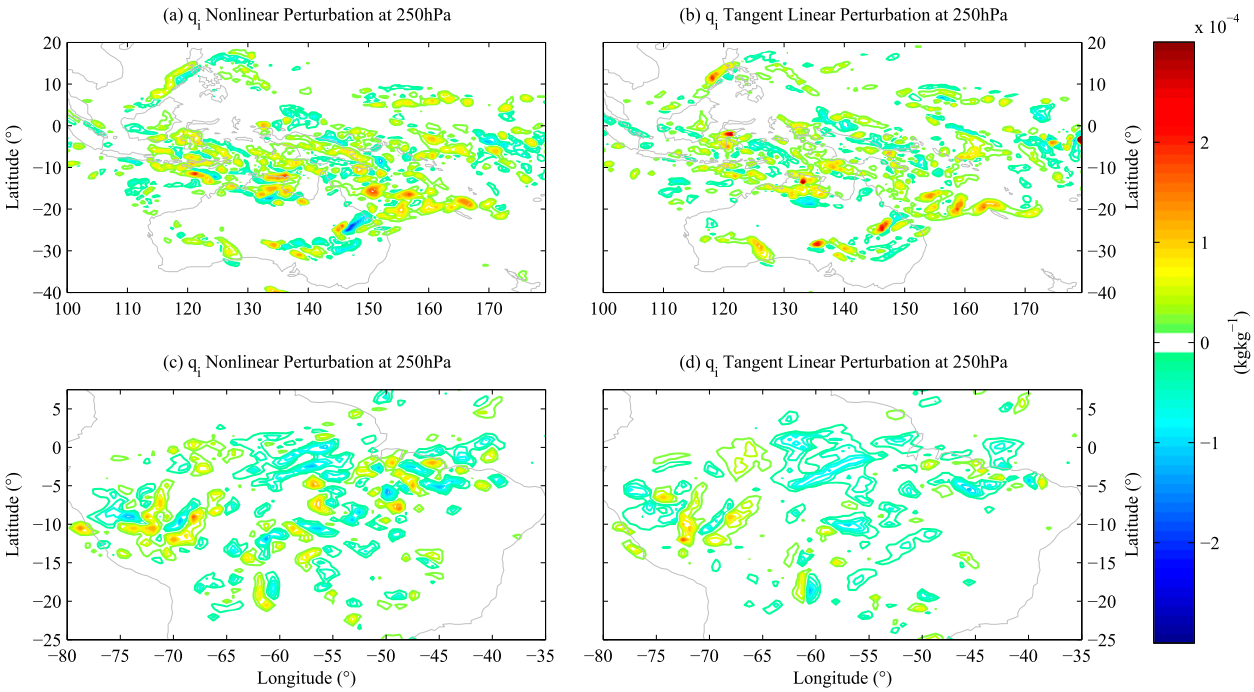


FIG. 7. As in Fig. 6, but showing the cloud liquid ice perturbation. (a),(b) The perturbations for a region of Australasia. (c),(d) A region over Brazil. The contour interval is $2 \times 10^{-5}$.

cloud liquid water perturbations, structure is captured in qualitatively similar locations and with similar magnitudes. Again there are some exceptions, where large-magnitude perturbations are only seen in either the nonlinear or linear perturbation trajectory. It is always difficult to capture the smallest-scale structures with the linearized model without also introducing other issues, such as spurious growth.

Although it is useful to examine certain levels and regions by eye, the correlation, RMSE, and RMS metrics provide a more quantitative impression of the performance of the tangent linear model. Figures 8a and 8b show the correlation for the cloud liquid water and cloud liquid ice, respectively. The metrics are computed for the 6-h forecast. The plot shows the correlations for both the tropics and globally. Note that correlations for clouds are quite low compared to the correlations seen in Fig. 5, for the reasons discussed in section 3b. It can be seen from Fig. 8a that the correlation for cloud liquid water reaches a minimum at around 850 hPa, the level shown in Fig. 6. For other levels examined by eye (not shown) more agreement is seen. Correlations for cloud liquid water increase to a maximum of approximately 0.6 at around 450 hPa. It is around these levels where cloud liquid water is forming as a result of convection. Correlations globally and for the tropics are similar at higher altitudes. Almost all clouds at these levels results from convection in the tropics.

Correlations for cloud liquid ice are fairly consistent between around 120 and 550 hPa and are between 0.4

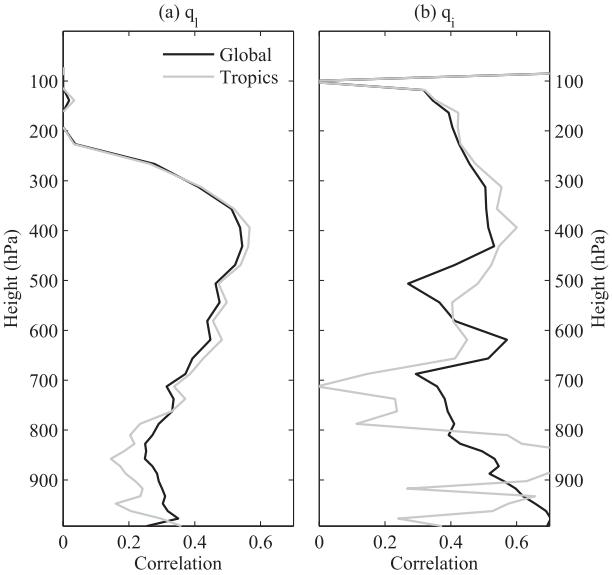


FIG. 8. Correlations between the linear and nonlinear perturbation trajectories for a 6-h forecast for (a) cloud liquid water and (b) cloud liquid ice.

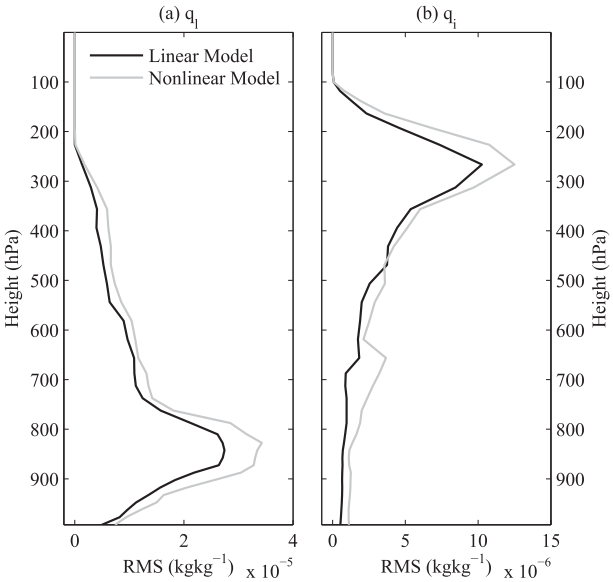


FIG. 9. The root-mean square of the (a) cloud liquid water perturbation and (b) cloud liquid ice perturbation.

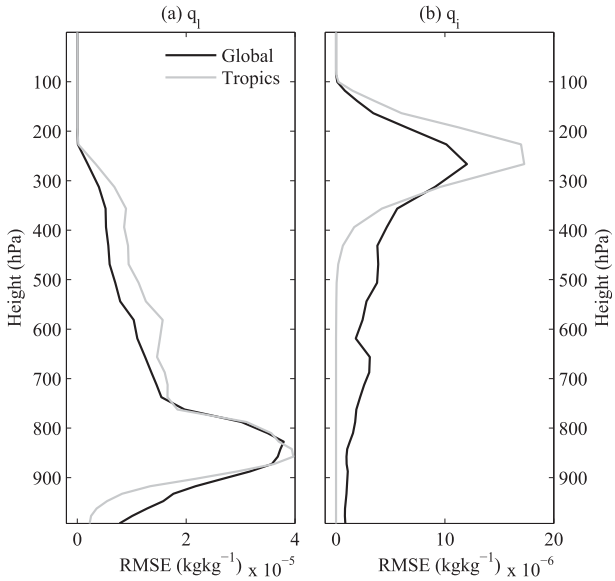


FIG. 10. As in Fig. 8, but showing the root-mean-square error in the linear perturbation trajectory.

and 0.5 globally. Outside of these levels minimal cloud liquid ice is present, especially in the tropics. Regions where perturbations are very sparse often results in somewhat erratic correlations. A few small phase or sign errors can result in zero and negative correlations. Likewise, the tangent linear model could get lucky in a few locations, giving small overall phase errors and a correlation near one.

Figures 9a and 9b show the global RMS for the cloud liquid water and cloud liquid ice for a 6-h forecast. The RMS provides an interpretation of the total magnitudes of each field so linear and nonlinear perturbation RMSs are shown as separate curves. For a perfect tangent linear model the two curves would lie on top of each other. It is clear that the magnitudes of the linear perturbations are similar to the nonlinear perturbations, but overall too small, as seen in the sparser horizontal structure earlier. Tuning of sources versus sinks in the linearized cloud scheme could be used to increase the RMS, but would also likely increase the RMSE and reduce the correlations. Much tuning has been used to optimize the performance of the cloud scheme, as measured in all the metrics.

Figures 10a and 10b show the RMSE for the cloud liquid water and cloud liquid ice for a 6-h forecast. Comparing Fig. 10 with Fig. 9 it is clear that the errors are largest at the levels where there is the most cloud cover. The RMSE for cloud liquid water perturbations increases slightly at high altitudes in the tropics, where there is relatively more cloud cover. Similarly RMSE for cloud liquid ice perturbations is lower in the tropics below 300 hPa where there is relatively less cloud cover. The RMSEs are reduced compared to treating the clouds as tracers in the tangent linear model (not shown). Note that the dry model only advects the initial conditions for clouds. As a result it lacks any physical relationship between the clouds and other thermodynamical variables so would not be useful in a data assimilation context, even if the errors did remain small.

All of the results so far demonstrate that convectively generated clouds have a greater degree of linearity than clouds formed through large-scale condensation. This can be seen by comparing high-level cloud ice water in the tropics with low-level cloud liquid water in the extratropics or globally. Correlations of cloud liquid ice are higher than for cloud liquid water and RMSEs of cloud liquid ice are smaller than for cloud liquid water. In addition, the fields appear qualitatively more similar in the horizontal plots. This result is as expected given the positive results seen for the linearized RAS convection scheme and the problems encountered when linearizing the PDF algorithm that is used for large-scale condensation. The sinks part of the cloud scheme uses a very similar algorithm for large-scale and anvil clouds. This further confirms that differences occur due to generation.

Unfortunately there is no way to model the perturbations produced by such a highly nonlinear model with complete accuracy. However, the results shown here demonstrate that a useful but also efficient linearization can be obtained. The window of both the 3DVAR and 4DVAR variational data assimilation systems at

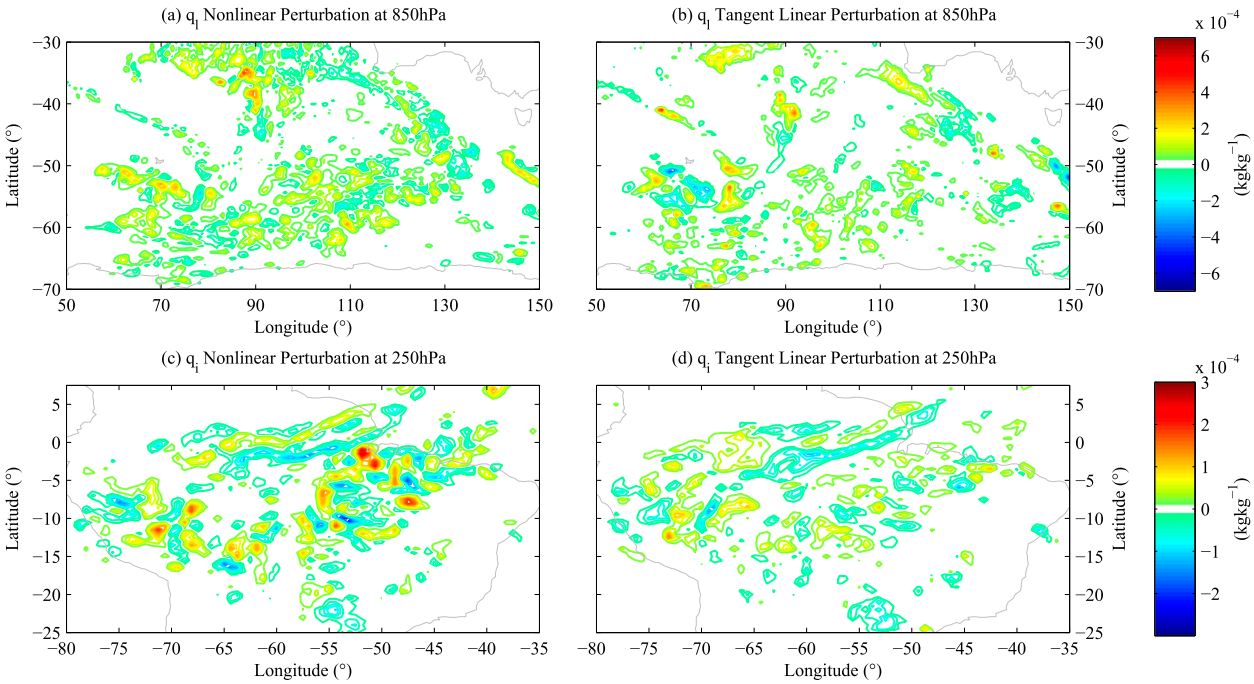


FIG. 11. As in Figs. 6a,b and Figs. 7c,d, but showing only $q_l$ and $q_i$ and for a 12-h integration.

GMAO is currently 6 h. Given these results, the linearized cloud model should prove useful for improving both of these systems and enable the development of the all-sky assimilation. Although there is currently no operational application, it is useful to also check the performance for a 12-h window. This informs for future expansions of the assimilation windows as well as increases confidence that any spurious perturbation growth is being well controlled. It should be noted that the scheme would be retuned if used for 12-h integrations, for example, by adjusting $\beta$ in Eq. (23).

Figure 11 shows horizontal cross sections for both cloud liquid water and cloud liquid ice perturbations for a 12-h forecast. Perturbations of cloud liquid water are shown for the region over the southern Indian Ocean and perturbations of cloud liquid ice are shown for the region over Brazil. This integration is a continuation of the integration used in Figs. 6–10. Comparing Figs. 11c and 11d it is seen that some of the cloud liquid ice perturbations are still well captured for this region. However, the difference between the linear and nonlinear perturbation trajectories is clearly increased over 6 h. Other regions have similar agreement (not shown). With retuning a greater degree of similarity could be achieved for 12 h and it is positive to note that the linearized model is not producing spuriously large perturbations for cloud liquid ice.

As seen at 6 h the cloud liquid ice perturbations are captured more accurately than cloud liquid water perturbations. In many locations the perturbations of cloud liquid water exist in the correct places; however, there are also regions where perturbations develop that should not be there and sign errors occur. For both the cloud liquid water and cloud liquid ice, regions that are clear of perturbations for the nonlinear model are also clear for the tangent linear model. The increased diffusion is clearly having more of an impact at 12 h, with perturbations of both cloud species thinning out compared to the nonlinear perturbations. Note that some of the largest perturbations seen at 6 h have not continued to develop and grow to 12 h, showing that the perturbation model is controlling spurious growth for the large-scale cloud generation.

The divergence between the nonlinear and linear perturbation trajectories compared to the difference at 6 h demonstrates the need for an alternative approach for longer runs.

### *e. Cloud scheme validation: 24-h forecasts*

The following analyzes the performance of the tangent linear model when using the cloud scheme with Jacobian filtering and tailored to longer integrations.

For observation impacts the cloud fields are not directly used in the calculation since they are not currently an observed quantity. Rather it is the winds, temperature, pressure, and specific humidity fields that are important. However, if clouds become an observed

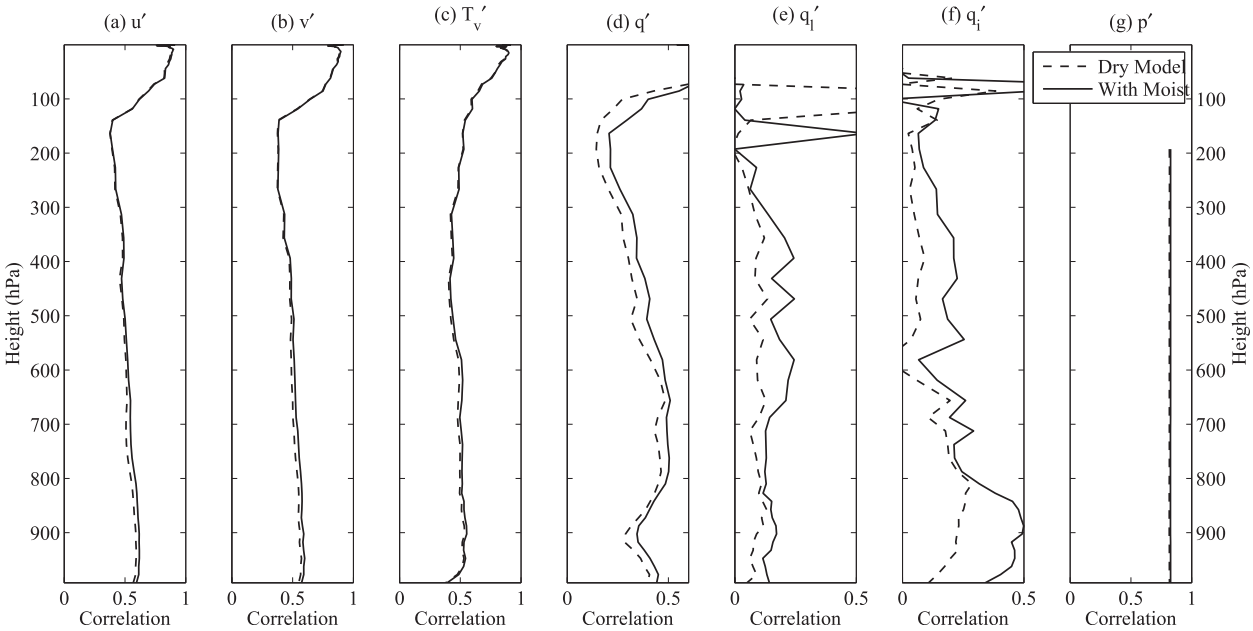


FIG. 12. Spatial correlations for a 24-h forecast. Correlations of (a) zonal wind $u'$, (b) meridional wind $v'$, (c) virtual temperature $T_v'$, (d) specific humidity $q'$, (e) cloud liquid water $q_l'$, (f) cloud liquid ice $q_i'$, and (g) pressure $p'$ (derived from surface pressure).

quantity then they could be included in the metric used for the calculation. Sensitivity to clouds may also be of interest in other research applications. For observation impacts it is important to check that the use of the linearized cloud model does not degrade another field, such as temperature, compared to running the model dry. Although this is not seen in the work here it may be an accepted drawback to gain the physical relationship between clouds and the other thermodynamic variables, and is a distinct possibility for a 24-h forecast.

Figure 12 shows the correlations for the tangent linear model for a 24-h forecast. The two sets of correlations are found when using the dry-physics-only tangent linear model and the moist physics tangent linear model. Correlations for the winds, temperature, and pressure are only slightly improved when using the moist physics. Improvement to the wind fields comes mainly from the convection scheme, rather than the cloud scheme. There is significant increase in the correlation of specific humidity. Although the dry-physics-only model simply advects the initial cloud perturbations, it is positive to note that the correlation in clouds improves when applying the new cloud scheme, even after 24 h. Nonlinearity in the cloud scheme could easily build up enough over 24 h to result in worsening the performance.

### *f. Quadrature method*

Here the performance of the Gaussian quadrature method is examined with the new linearized cloud scheme. There is no way to fairly measure the performance of the Gaussian quadrature using only the tangent linear model. By linearizing about the average of two trajectories more information about the specific chosen perturbation is provided. Comparing with the single trajectory used so far would not be fair. Instead the perturbation is integrated along both analysis and background trajectories, the resulting perturbations are averaged and then compared with the result of using the Gaussian quadrature. This provides a slightly fairer comparison and mimics what is done for observation impacts. Although this does not provide a true measure of the performance of the Gaussian quadrature, it is a useful to check that the method performs broadly as expected when the cloud scheme is being employed.

Figure 13 shows the perturbation correlations for a 24-h forecast for temperature (Fig. 13a), specific humidity (Fig. 13b), cloud liquid water (Fig. 13c), and cloud liquid ice (Fig. 13d). The figure shows the correlations when averaging the result of integrating along both trajectories versus using the Gaussian quadrature approach. In all cases the full linearized moist physics schemes with filtering are active. It is clear that the use of the Gaussian quadrature approach improves the solution, as expected. Similar results have also been noted for shorter forecasts and using the perturbation model cloud scheme (not shown). Examining other metrics and configurations, it is clear that the Gaussian quadrature generally controls the development of unrealistically large perturbations where they may otherwise be present (not shown).

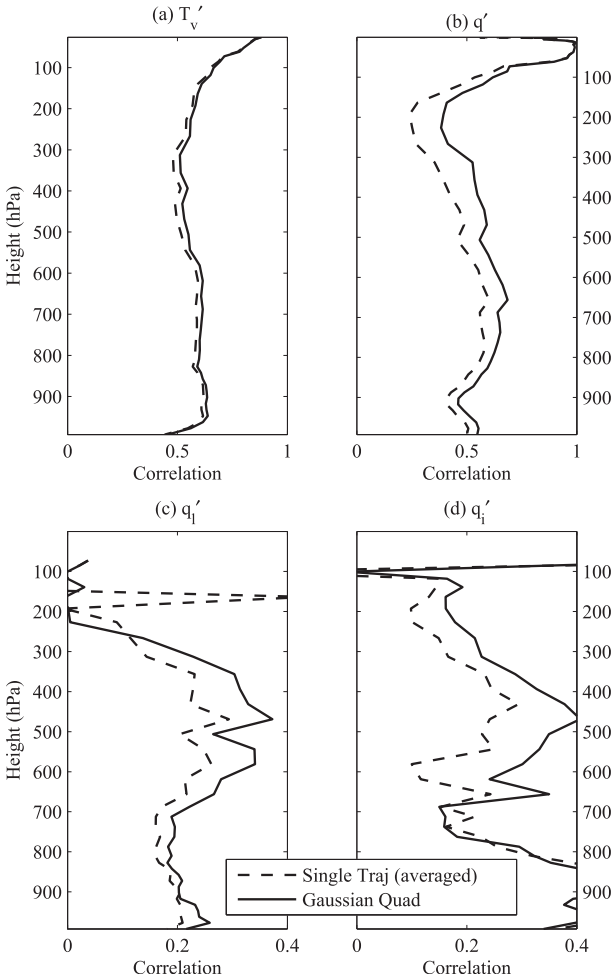


FIG. 13. Correlations for a 24-h forecast when averaging the results of linearizing around the analysis and background trajectories and when using Gaussian quadrature.

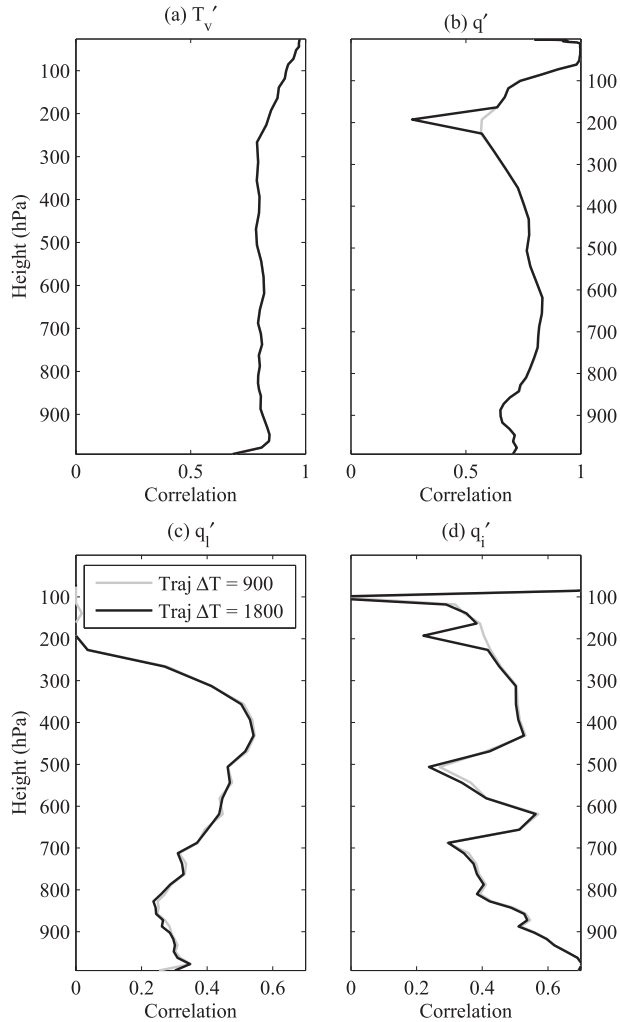


FIG. 14. Correlations for a 6-h forecast when using the normal trajectory read frequency and a reduced frequency.

### g. *Reduced trajectory read frequency*

The storing of the trajectory used by the linearized model can be rather memory intensive and reading the data rather time consuming. Instead of storing and reading the trajectory for every time step of the linearized model, it can be read every other time step or even every four time steps. For the dry-physics-only linearized model a reduction to every four time steps can be used without having a negative effect on the performance.

Figure 14 shows the correlations for a 6-h forecast when using the perturbation model and two different frequencies of trajectory read: 900 and 1800 s. For this 6-h forecast the effect of reducing the frequency of the trajectory is fairly minimal. However, at the 200-hPa level the correlations are starting to suffer. The same experiment has been performed for longer integration times and using the filtering method. In that case reducing the read frequency to 1800 s negatively impacted the results and significantly reduced the correlations (not shown). The moist physics relies heavily on switches in the numerical code. For example, convection is either on or off, evaporation is either on or off, etc. These switches are determined by values in the trajectory. By reducing the frequency of the trajectory, these switches will become less representative of the nonlinear model and cause the linear perturbation trajectory to diverge from the nonlinear perturbation trajectory. Further, if a growing structure occurs in a grid box then the structure of that mode would be repeated at the subsequent time step, causing a more rapid growth of the perturbation.

## 4. Summary

A linearized prognostic cloud scheme has been developed and implemented in NASA's GEOS-5 data

assimilation tools. The main motivations for developing this scheme are to provide a framework for assimilating observations of clouds in the GSI and to improve observation impacts.

The linearization of the cloud scheme is derived directly from the cloud scheme used in the nonlinear model. This approach is chosen so as to maximize the similarity between the nonlinear and linear perturbation trajectories and to easily tie in the already developed linearized convection scheme. Generally the nonlinear cloud scheme has good linearity properties and does not employ many functions with steep gradients. The exception to this is the part of the scheme that models the formation of clouds through so-called large-scale condensation. The approach centers around determining the area of a PDF of gridbox total water that corresponds to supersaturation. Nonlinearity and rapid perturbation growth is intrinsic in the algorithm, particularly in the formulation of cloud fraction. Linearizing this part of the scheme in its standard form does not produce realistic results.

The main requirement when using the linearized model for data assimilation is efficiency, while for observation impacts it is accuracy over a longer window. Given these two distinct requirements, two approaches to handling the problems of the cloud fraction formulation have been developed. For the data assimilation applications a perturbation model for cloud fraction is developed. Instead of using the PDF, the cloud fraction is given by a simplified piecewise linear function and the gradient of that function is regularized. This approach was tested in the nonlinear model and gave very similar cloud cover. Over a longer window the perturbation model approach causes the linear and nonlinear perturbation trajectories to diverge, perturbation growth is too large, and in the wrong locations. For the longer lead times a filtering has been developed. This filtering computes the Jacobian of just the part of the cloud model that handles large-scale condensation. By examining the Jacobian elements as well as its eigenvalues it is possible to determine when the linearization of the standard PDF approach is well behaved. By only invoking the perturbation model for grid boxes that encounter a problem it is possible to maintain accuracy over the longer window.

Through a variety of metrics it is demonstrated that the linearized cloud model performs well. The location of nonlinear cloud perturbations are often well captured by the tangent linear model and the problems around cloud fraction are controlled. Generally the cloud perturbations that occur as a result of convection are better represented than those formed as a result of large-scale condensation. For example, cloud liquid ice perturbations at heights around 250 hPa are consistently captured more accurately than cloud liquid water perturbations at heights around 850 hPa. The way convection is modeled in GEOS-5 is generally more linear than the way large-scale condensation is modeled. Large-scale condensation is modeled using a discrete switch at the point of supersaturation, which is an equilibrium point. The constant proximity to the switch results in a buildup of nonlinearity.

Other than in the sources, the algorithms for large-scale clouds and anvil clouds are very similar. That perturbations of clouds produced by convection are well represented shows that the evaporation, autoconversion, and precipitation parts of the cloud model have good linearity properties. The problems are really centered around the large-scale condensation. Extensive effort went into understanding these issues and many different approaches were tested in an attempt to maximize the performance of the linearized model. The combination of using the perturbation model and filtering produces the best compromise of realistic perturbation growth, linearity, and accuracy for the required lead times. Even for 24-h forecasts the approach provides sensible cloud perturbations and the capturing of specific humidity and cloud variables is significantly improved over using a dry-physics-only model. Throughout this work it has been noted that the linearized model is generally too diffusive, especially for clouds. This is a compromise that is required to obtain a linearized model that performs well overall and is reliable for multiple different applications.

The linearized cloud model is also examined with two alternative approaches to the handling of the trajectory of reference variables. First using Gaussian quadrature to provide an averaged trajectory, and second reducing the frequency of the trajectory read. For Gaussian quadrature the linearized cloud model performs well and improvement over using the normal trajectories was noted. For 6-h forecasts the trajectory read frequency could be reduced to 1800 s without adversely impacting the capturing of cloud and thermodynamic perturbations. For longer integrations reducing the frequency significantly degraded the results. Not having the trajectory at the correct time places the moist physics schemes into the wrong regime, evaporation or convection occurring where it normally would not be for example.

As a result of developing the linearized cloud scheme, it was noted that the schemes used for dynamical advection in GEOS-5 are highly nonlinear and can exhibit perturbation growth. These problems are particularly bad when the field being advected contains discontinuities, which is certainly the case for clouds.

Rather than handling the advection of cloud and specific humidity perturbations using these high-order nonlinear schemes, they have been replaced with a simple linearized third-order scheme. This prevents the growth of perturbations and improves linearity, but slightly reduces the perturbation magnitudes overall. It is worth investigating these findings further so as to understand why certain flux limiters support perturbation growth and to determine whether some form of flux limiter can be used in a linearized model without such poor behavior.

*Acknowledgments.* This work is funded under the NASA-USRA GESTAR cooperative agreement. Thanks to Andrea Molod of GMAO for assistance in deciphering the cloud model code.

## REFERENCES

Amerault, C., X. L. Zou, and J. Doyle, 2008: Tests of an adjoint mesoscale model with explicit moist physics on the cloud scale. *Mon. Wea. Rev.*, **136**, 2120–2132, doi:10.1175/2007MWR2259.1.

Arakawa, A., and W. H. Schubert, 1974: Interaction of a cumulus cloud ensemble with the large-scale environment, Part I. *J. Atmos. Sci.*, **31**, 674–701, doi:10.1175/1520-0469(1974)031<0674:IOACCE>2.0.CO;2.

Bacmeister, J., M. Suarez, and F. R. Robertson, 2006: Rain reevaporation, boundary layer–convection interactions, and Pacific rainfall patterns in an AGCM. *J. Atmos. Sci.*, **63**, 3383–3403, doi:10.1175/JAS3791.1.

Bloom, S. C., L. L. Takacs, A. M. da Silva, and D. Ledvina, 1996: Data assimilation using incremental analysis updates. *Mon. Wea. Rev.*, **124**, 1256–1271, doi:10.1175/1520-0493(1996)124<1256:DAUIAU>2.0.CO;2.

Charpentier, I., 2001: Checkpointing schemes for adjoint codes: Application to the meteorological model Meso-NH. *SIAM J. Sci. Comput.*, **22**, 2135–2151, doi:10.1137/S1064827598343735.

Claerbout, J., 2014: *Geophysical Image Estimation by Example*. lulu.com, 252 pp.

Ehrendorfer, M., and R. Errico, 1995: Mesoscale predictability and the spectrum of optimal perturbations. *J. Atmos. Sci.*, **52**, 3475–3500, doi:10.1175/1520-0469(1995)052<3475:MPATSO>2.0.CO;2.

Errico, R., and K. Raeder, 1999: An examination of the accuracy of the linearization of a mesoscale model with moist physics. *Quart. J. Roy. Meteor. Soc.*, **125**, 169–195, doi:10.1002/qj.49712555310.

——, P. Bauer, and J.-F. Mahfouf, 2007: Issues regarding the assimilation of cloud and precipitation data. *J. Atmos. Sci.*, **64**, 3785–3798, doi:10.1175/2006JAS2044.1.

Gelaro, R., R. Langland, S. Pellerin, and R. Todling, 2010: The THORPEX observation impact intercomparison experiment. *Mon. Wea. Rev.*, **138**, 4009–4025, doi:10.1175/2010MWR3393.1.

——, R. Mahajan, and R. Todling, 2014: Observation impacts for longer forecast lead-times. *18th Conf. on Integrated Observing and Assimilation Systems for the Atmosphere, Oceans, and Land Surface (IOAS-AOLS)*, Atlanta, GA, Amer. Meteor. Soc., 1.1. [Available online at https://ams.confex.com/ams/94Annual/webprogram/Paper234632.html.]

Holdaway, D., and R. Errico, 2014: Using Jacobian sensitivities to assess a linearisation of the relaxed Arakawa–Shubert convection scheme. *Quart. J. Roy. Meteor. Soc.*, **140**, 1319–1332, doi:10.1002/qj.2210.

——, J. Thuburn, and N. Wood, 2013: Comparison of Lorenz and Charney–Phillips vertical discretisations for dynamics–boundary layer coupling. Part II: Transients. *Quart. J. Roy. Meteor. Soc.*, **139**, 1087–1098, doi:10.1002/qj.2017.

——, R. Errico, R. Gelaro, and J. G. Kim, 2014: Inclusion of linearized moist physics in NASA's Goddard Earth Observing System data assimilation tools. *Mon. Wea. Rev.*, **142**, 414–433, doi:10.1175/MWR-D-13-00193.1.

Hou, A. Y., G. Skofronick-Jackson, C. D. Kummerow, and J. M. Shepherd, 2008: Global precipitation measurement. *Precipitation: Advances in Measurement, Estimation and Prediction*, S. C. Michaelides, Ed., Springer, 131–169.

Janisková, M., J. Thépaut, and J.-F. Geleyn, 1999a: Simplified and regular physical parameterizations for incremental four-dimensional variational assimilation. *Mon. Wea. Rev.*, **127**, 26–45, doi:10.1175/1520-0493(1999)127<0026:SARPPF>2.0.CO;2.

——, F. Veersé, J.-N. Thépaut, G. Desroziers, and B. Pouponneau, 1999b: Impact of a simplified physical package in 4D-var analyses of FASTEX situations. *Quart. J. Roy. Meteor. Soc.*, **125**, 2465–2485, doi:10.1002/qj.49712555907.

Jung, B.-J., and H. M. Kim, 2009: Moist adjoint-based forecast sensitivities for a heavy snowfall event over the Korean Peninsula on 4–5 March 2004. *J. Geophys. Res.*, **114**, D15104, doi:10.1029/2008JD011370.

——, ——, T. Auligné, X. Zhang, X. Zhang, and X.-Y. Huang, 2013: Adjoint-derived observation impact using WRF in the western North Pacific. *Mon. Wea. Rev.*, **141**, 4080–4097, doi:10.1175/MWR-D-12-00197.1.

Langland, R., and N. Baker, 2004: Estimation of observation impact using the NRL atmospheric variational data assimilation adjoint system. *Tellus*, **56A**, 189–201, doi:10.1111/j.1600-0870.2004.00056.x.

Lawrence, M. G., and P. J. Crutzen, 1998: The impact of cloud particle gravitational settling on soluble trace gas distributions. *Tellus*, **50B**, 263–289, doi:10.1034/j.1600-0889.1998.t01-2-00005.x.

Lin, S.-J., 2004: A "vertically Lagrangian" finite-volume dynamical core for global models. *Mon. Wea. Rev.*, **132**, 2293–2307, doi:10.1175/1520-0493(2004)132<2293:AVLFDC>2.0.CO;2.

Lopez, P., and E. Moreau, 2005: A convection scheme for data assimilation: Description and initial tests. *Quart. J. Roy. Meteor. Soc.*, **131**, 409–436, doi:10.1256/qj.04.69.

Lorenc, A. C., and R. T. Marriott, 2014: Forecast sensitivity to observations in the Met Office global numerical weather prediction system. *Quart. J. Roy. Meteor. Soc.*, **140**, 209–224, doi:10.1002/qj.2122.

Mahfouf, J.-F., and F. Rabier, 2000: The ECMWF operational implementation of four-dimensional variational assimilation. II: Experimental results with improved physics. *Quart. J. Roy. Meteor. Soc.*, **126**, 1171–1190, doi:10.1002/qj.49712656416.

Molod, A., 2012: Constraints on the profiles of total water PDF in AGCMs from AIRS and a high-resolution model. *J. Climate*, **25**, 8341–8352, doi:10.1175/JCLI-D-11-00412.1.

Moorthi, S., and M. J. Suarez, 1992: Relaxed Arakawa–Schubert: A parameterization of moist convection for general circulation models. *Mon. Wea. Rev.*, **120**, 978–1002, doi:10.1175/1520-0493(1992)120<0978:RASAPO>2.0.CO;2.

Polavarapu, S., and M. Tanguay, 1998: Linearizing iterative processes for four-dimensional data-assimilation schemes. *Quart. J. Roy. Meteor. Soc.*, **124**, 1715–1742, doi:10.1002/qj.49712454917.

Slingo, J. M., and B. Ritter, 1985: Cloud prediction in the ECMWF model. Tech. Rep. 46, ECMWF, 49 pp.

Smith, R. N. B., 1990: A scheme for predicting layer clouds and their water content in a general circulation model. *Quart. J. Roy. Meteor. Soc.*, **116**, 435–460, doi:10.1002/qj.49711649210.

Stappers, R. J. J., and J. Barkmeijer, 2013: Gaussian quadrature 4D-Var. *Quart. J. Roy. Meteor. Soc.*, **139**, 1462–1472, doi:10.1002/qj.2056.

Stiller, O., 2009: Efficient moist physics schemes for data assimilation. II: Deep convection. *Quart. J. Roy. Meteor. Soc.*, **135**, 721–738, doi:10.1002/qj.362.

——, and S. P. Ballard, 2009: Efficient moist physics schemes for data assimilation. I: Large-scale clouds and condensation. *Quart. J. Roy. Meteor. Soc.*, **135**, 707–720, doi:10.1002/qj.400.

Thuburn, J., and T. W. N. Haine, 2001: Adjoints of nonoscillatory advection schemes. *J. Comput. Phys.*, **171**, 616–631, doi:10.1006/jcph.2001.6799.

Tiedtke, M., 1993: Representation of clouds in large-scale models. *Mon. Wea. Rev.*, **121**, 3040–3061, doi:10.1175/1520-0493(1993)121<3040:ROCILS>2.0.CO;2.

Tompkins, A. M., and M. Janiskova, 2004: A cloud scheme for data assimilation: Description and initial tests. *Quart. J. Roy. Meteor. Soc.*, **130**, 2495–2517, doi:10.1256/qj.03.162.